Investigating the color-suppressed decays $\Lambda_b \to \Lambda\psi$ in the perturbative QCD approach

Zhou Rui,* Chao-Qi Zhang, Jia-Ming Li, and Meng-Kun Jia

College of Sciences, North China University of Science and Technology, Tangshan 063009, China

(Received 13 June 2022; accepted 31 August 2022; published 22 September 2022)

The nonleptonic two-body $\Lambda_b \to \Lambda\psi$ decays with $\psi = J/\psi$ or $\psi(2S)$ are investigated based on the perturbative QCD approach. These are color-suppressed processes in which the nonfactorizable contributions are confirmed to be dominant. Angular momentum conservation allows us to describe the concerned decays by four independent complex helicity amplitudes. It is observed that the negative-helicity states for the Λ baryon are preferred as expected in the left-handed nature of the charged-current interaction. The obtained results for the helicity amplitudes are used to compute the branching ratios and various observable parameters, which are then compared to the existing theoretical predictions and experimental data. In particular, we predict the ratio $\mathcal{R} = \frac{\mathcal{B}(\Lambda_b \to \Lambda\psi(2S))}{\mathcal{B}(\Lambda_b \to \Lambda J/\psi)} = 0.47^{+0.02}_{-0.00}$ in comparison with 0.508 ± 0.023 from the Particle Data Group at the level of 1 standard deviation. We also briefly explore the long-distance contributions to the semileptonic $\Lambda_b \to \Lambda l^+ l^-$ decays in the kinematic regions where the dilepton invariant masses are around the J/ψ and $\psi(2S)$ resonances.

DOI: 10.1103/PhysRevD.106.053005

I. INTRODUCTION

Exclusive decays of b-flavored hadrons into charmonia, governed by the weak $b \to sc\bar{c}$ transition, provide valuable insight into the dynamics of strong interactions in the heavy hadronic decays. The charmonium mode belongs to the color-suppressed category [1], which receives large nonfactorizable contributions and poses a challenge for the factorization ansatz. Such processes have been the subject of theoretical and experimental interest in bottom meson decays, such as $B \to J/\psi K$ [2–6]. In the baryon sector, the typical process is the $\Lambda_b \to \Lambda J/\psi$ decay, where the QCD dynamics are more complicated by the presence of extra spectator quarks. As Λ_b has nonzero spin, this mode is a useful environment in which to study the helicity structure of the underlying Hamiltonian [7–9].

The b-hadron decays into J/ψ are experimentally convenient because the subsequent decay $J/\psi \to \mu^+\mu^-$ has particularly distinctive signatures. The $\Lambda_b \to \Lambda J/\psi$ mode was first observed by the UA1 Collaboration at the CERN proton-antiproton ($p\bar{p}$) collider [10], followed by extensive studies at the Fermilab Tevatron by the CDF [11–13] and D0 [14–17] Collaborations. However, its absolute branching ratio has not yet been determined, since the experimental knowledge of the fraction of b quarks which hadronize to Λ_b baryons is currently limited. The current Particle Data Group (PDG) presents an average value [18]

$$f(b \to \Lambda_b) \times \mathcal{B}(\Lambda_b \to \Lambda J/\psi) = (5.8 \pm 0.8) \times 10^{-5}, \quad (1)$$

where $f(b \to \Lambda_b)$ describes the probability that a b quark fragments into a Λ_b baryon. Another salient feature of the decay is the wealth of information carried by angular observables in terms of angular asymmetries that can be exploited to probe new physics beyond the standard model. An angular analysis of the decay $\Lambda_b \to \Lambda J/\psi$ was first done by the LHCb Collaboration [19], where the Λ_b's are produced in pp collisions at the Large Hadron Collider (LHC). Subsequently, a similar analysis was also performed by the ATLAS [20] and CMS [21,22] Collaborations. Some interesting observables, such as the helicity amplitudes, production polarization, the parity-violating parameter and other asymmetry parameters, are now available. A latest analysis was conducted by the LHCb Collaboration [23], in which the polarization of Λ_b baryons is measured for the first time at $\sqrt{s} = 13$ TeV. All of these measurements show that the production polarization of Λ_b is consistent with zero.

As a tremendous amount of beauty baryons is produced at the LHC, numerous decays of the Λ_b baryon to excited charmonium states have been observed [24–27]. Among these, the decay mode $\Lambda_b \to \Lambda\psi(2S)$ is of particular interest

*Corresponding author.
jindui1127@126.com

because it is the radial excited partner of $\Lambda_b \to \Lambda J/\psi$ with the same topology. It could provide additional and complementary phenomenological information on the QCD dynamics of the charmonium Λ_b decays. The first observation of $\Lambda_b \to \Lambda\psi(2S)$ was made by the ATLAS Collaboration [28]. Later, the reaction was also observed by the LHCb Collaboration [29]. Similarly, no absolute branching ratio is measured for this decay, and only ratios to other reactions are provided. Its branching ratio relative to the J/ψ mode given by the PDG is $\mathcal{B}(\Lambda_b \to \Lambda\psi(2S))/\mathcal{B}(\Lambda_b \to \Lambda J/\psi) = 0.508 \pm 0.023$ [18], which was deduced from the measurements by the ATLAS [28] and LHCb [29] Collaborations. This result was lower than similar measurements in the B systems, such as $\mathcal{B}(B^0 \to \psi(2S)K^0)/\mathcal{B}(B^0 \to J/\psi K^0) = 0.82 \pm 0.18$ [18] and $\mathcal{B}(B^+ \to \psi(2S)K^+)/\mathcal{B}(B^+ \to J/\psi K^+) = 0.611 \pm 0.019$ [18]. Since the uncertainty due to hadronic effects cancels to a large extent, a comparison of the beauty meson and baryon branching ratios can be used to test the factorization of amplitudes and provide useful information on the production of charmonia in b-hadron decays.

These observations motivate us to investigate the dynamics of the charmonium modes in the baryon sector. Particularly, the decays $\Lambda_b \to \Lambda J/\psi, \Lambda\psi(2S)$ are quite appealing from a theoretical point of view in that they proceed solely via W-emission diagrams, and there is no contribution due to W-exchange diagrams [30]. Meanwhile, similar to the mesonic analog, a significant impact of nonfactorizable contributions is expected, which provides valuable additional information to improve our understanding of the nonfactorizable mechanism. There have been a number of theoretical calculations for the decays under study in the literature [31–48]. Very recently, the angular distributions for the decays $\Lambda_b \to \Lambda^* J/\psi$, where the Λ^* are Λ-type excited states, have been derived by using the helicity amplitude technique [49]. They calculated the partial decay width, polarization, and forward-backward asymmetry.

From a theoretical point of view, one difficult thing is to evaluate the hadronic matrix element of local operators between the initial and final states, which require nonperturbative hadronic inputs. The perturbative QCD factorization (PQCD) approach can serve as a useful tool for investigating the heavy baryon decays. The basic ingredient is that the decay amplitude is factorized into the convolution of the hard kernel, the jet functions with the universal nonperturbative wave functions. The jet functions organize double logarithms appearing in the hard kernel, whose resummation gives the Sudakov factor and guarantees the removal of the end point singularities. The PQCD approach has been developed and successfully applied to deal with various decays of a Λ_b baryon [38,50–56]. We recently have analyzed the nonleptonic decays of $\Lambda_b \to \Lambda_c \pi, \Lambda_c K$ by using the PQCD approach and obtained satisfactory results. This work focuses on the study of $\Lambda_b \to \Lambda J/\psi$, $\Lambda\psi(2S)$ decays. The former have been studied in a previous work [38] compared to which the analysis and scope of this work is improved in several aspects.

The Λ_b baryon light-cone distribution amplitudes (LCDAs) are included up to the twist-4 level according to the general Lorentz structures in Refs. [57–60]. The LCDAs of a Λ baryon are taken from QCD sum rules [61] at leading-twist accuracy. For the LCDAs of the charmonium states, we adopt the harmonic oscillator models proposed in our previous work [62,63], which are successful in describing various hadronic charmonium B and B_c decays [64–72]. Thus, we are motivated to check for the validity of the same scenario in the baryon sector. It is worth emphasizing that here we distinguish the LCDAs of the charmonia for the longitudinal and transverse polarizations since they exhibit different asymptotic behaviors. In particular, the twist-3 ones contribute to the decay amplitude through the nonfactorization diagrams and play an important role in the concerned color-suppressed decays. For the Sudakov factor of the charmonium states, we employ the recent updated results from Refs. [73,74], which were derived at the next-to-leading-logarithmic accuracy by including the effect from charm quark mass. Finally, similar to the cases of hadronic charmonium B meson decays, we also consider the vertex corrections to the factorizable amplitudes at the current known next-to-leading-order level, whose effects can be combined in the Wilson coefficients as usual [75–77]. In addition, the corresponding $\psi(2S)$ channel is also investigated, which is helpful to test the factorization by its relative branching ratio as mentioned before. Besides the decay branching ratios, many asymmetries derived from helicity amplitudes are also predicted and compared with currently available theoretical predictions and experiments.

We present our work as follows: In Sec. II, we give a brief description of the theoretical framework underlying the formulation of the PQCD, such as kinetic conventions, hadronic LCDAs, and the effective Hamiltonian. Thereafter, the numerical results for the transition form factors, invariant and helicity amplitudes, decay branching ratios, up-down asymmetries, and other pertinent decay asymmetry parameters are presented in Sec. III. We end with a brief summary in Sec. IV. Appendixes A and B are prepared to give some details of the Λ_b LCDAs and factorization formulas, respectively.

II. THEORETICAL FRAMEWORK

As already mentioned, the concerned decays only receive the contributions from the W-emission diagrams, in which the two spectator quarks are shared by the parent and daughter baryons Λ_b and Λ, respectively. In the PQCD framework, the perturbative calculations start at the order of $\mathcal{O}(\alpha_s^2)$. The related Feynman diagrams at the leading order level are shown in Fig. 1. Following the same convention in Ref. [56], each diagram is denoted by T_{ij} with subscripts

$i = a - f$ and $j = 1$–7 representing the possible ways of exchanging two hard gluons. The factorizable diagrams correspond to $a1 - a5$, $b1 - b5$, $e1, e2$, and $f1, f2$, while the remaining ones are all classified as nonfactorizable ones. The triple-gluon vertex diagrams do not contribute since the corresponding color rearrangement factors are zero in the present case.

It is convenient to work in the rest frame of the parent baryon Λ_b with the daughter baryon Λ moving in the positive direction on the light cone such that $p = \frac{M}{\sqrt{2}}(1, 1, \mathbf{0}_T)$ and $p' = \frac{M}{\sqrt{2}}(f^+, f^-, \mathbf{0}_T)$ with M being the Λ_b baryon mass. Then, the momentum (q) and the longitudinal and transverse polarization vectors ($\epsilon_{L,T}$) of the charmonium can be determined by the momentum conservation and the normalization and orthogonality conditions as

$$\begin{aligned} q &= \frac{M}{\sqrt{2}}(1 - f^+, 1 - f^-, \mathbf{0}_T), \\ \epsilon_L &= \frac{1}{\sqrt{2}r}(f^+ - 1, 1 - f^-, \mathbf{0}_T), \\ \epsilon_T &= (0, 0, \mathbf{1}_T), \end{aligned} \tag{2}$$

where the factors

$$f^{\pm} = \frac{1}{2}(1 - r^2 + r_\Lambda^2 \pm \sqrt{(1 - r^2 + r_\Lambda^2)^2 - 4r_\Lambda^2}), \tag{3}$$

with the mass ratio $r_{(\Lambda)} = m_{(\Lambda)}/M$, and $m_{(\Lambda)}$ is the mass of the charmonium (Λ baryon). The momenta of eight quarks as shown in Fig. 1 are parametrized as

$$\begin{aligned} k_1 &= \left(\frac{M}{\sqrt{2}}, \frac{M}{\sqrt{2}}x_1, \mathbf{k}_{1T}\right), \quad k_2 = \left(0, \frac{M}{\sqrt{2}}x_2, \mathbf{k}_{2T}\right), \\ k_3 &= \left(0, \frac{M}{\sqrt{2}}x_3, \mathbf{k}_{3T}\right), \quad k_1' = \left(\frac{M}{\sqrt{2}}f^+x_1', 0, \mathbf{k}_{1T}'\right), \\ k_2' &= \left(\frac{M}{\sqrt{2}}f^+x_2', 0, \mathbf{k}_{2T}'\right), \quad k_3' = \left(\frac{M}{\sqrt{2}}f^+x_3', 0, \mathbf{k}_{3T}'\right), \\ q_1 &= \left(\frac{M}{\sqrt{2}}y(1 - f^+), \frac{M}{\sqrt{2}}y(1 - f^-), \mathbf{q}_T\right), \\ q_2 &= \left(\frac{M}{\sqrt{2}}(1 - y)(1 - f^+), \frac{M}{\sqrt{2}}(1 - y)(1 - f^-), -\mathbf{q}_T\right), \end{aligned} \tag{4}$$

where $x_{1,2,3}$, $x'_{1,2,3}$, and y are the parton longitudinal momentum fractions and $\mathbf{k}_{1T,2T,3T}$, $\mathbf{k}'_{1T,2T,3T}$, and $\mathbf{q}_T$ are the corresponding transverse momenta. They satisfy the momentum conservation condition:

$$\sum_{l=1}^{3} x_l = 1, \qquad \sum_{l=1}^{3} \mathbf{k}_{lT} = 0. \tag{5}$$

A similar argument holds for the primed quantities. Here, only the heavy b and c quark masses are kept, while other light quarks are treated as massless. This means only one of the dominant components of k_i' and $k_{2,3}$ is kept so that $k^2 = m^2 \approx 0$ in the massless limit. Since k_i' are aligned with the Λ baryon in the dominant plus direction, their small minus components have been neglected. The minus components of k_2 and k_3 for the soft light quarks on the Λ_b baryon side are selected by their inner products with k_i', which appear in the hard-kernel calculations for the concerned processes.

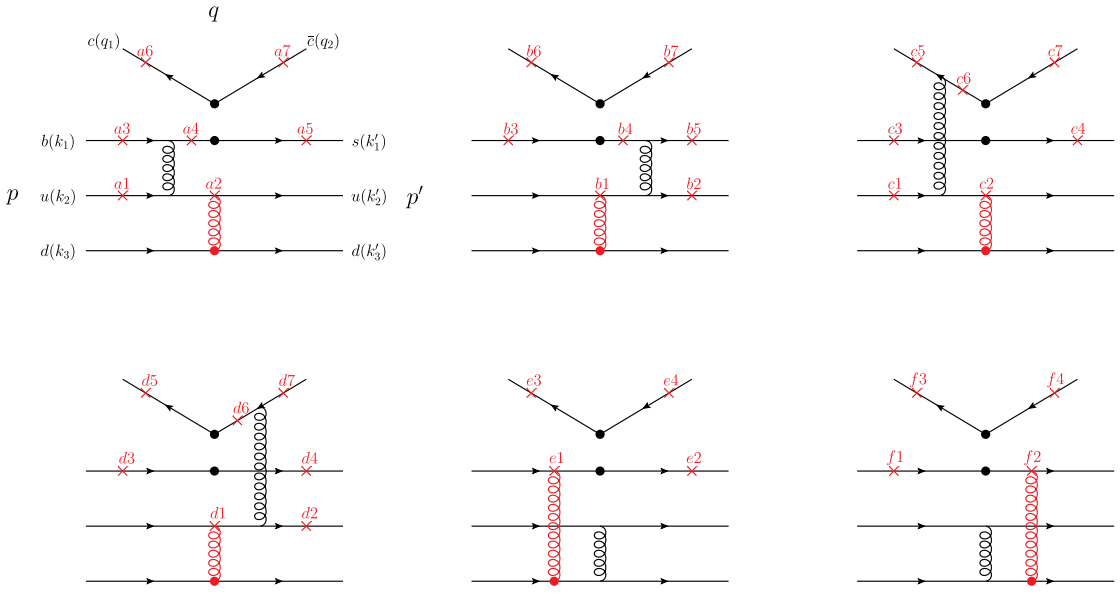

FIG. 1. Feynman diagrams for the $\Lambda_b \to \Lambda J/\psi$ decay at the leading order, where the solid black dot represents the vertex of the effective weak interaction. The crosses on the quark lines indicated by ij with $i = a - f$ and $j = 1$–7 denote the possible ways in which the quark is connected to the spectator d quark via a hard gluon.

As the fast recoiled Lambda baryon moves approximately in the plus direction, $f^- \sim \mathcal{O}(m_\Lambda^2/M^2)$ is a small quantity, and the sum of k_i' equal to p' holds approximately.

In the course of the PQCD calculations, the necessary inputs contain the hadronic LCDAs of the initial and final states, which can be constructed via the nonlocal matrix elements. We next specify the relevant LCDAs for the present study. After the complete classification of the three-quark LCDAs of the Λ_b baryon in the heavy-quark limit was constructed [58], the investigation of the Λ_b baryon wave function has made great progress in the last decade [57–60,78,79]. Its explicit form up to twist-4 in the momentum space can be written as [55]

$$(\Psi_{\Lambda_b})_{\alpha\beta\gamma}(x_i,\mu) = \frac{1}{8\sqrt{2}N_c}\{f^{(1)}_{\Lambda_b}(\mu)[M_1(x_2,x_3)\gamma_5 C^T]_{\gamma\beta} + f^{(2)}_{\Lambda_b}(\mu)[M_2(x_2,x_3)\gamma_5 C^T]_{\gamma\beta}\}[\Lambda_b(p)]_\alpha, \tag{6}$$

where α, β, γ are the spinor indices. $\Lambda_b(p)$ is the heavy baryon spinor with the quantum number $I(J^P) = 0(\frac{1}{2}^+)$. N_c is the number of colors. C^T denotes the charge conjugation matrix under transpose transform. The normalization constants $f^{(1)}_{\Lambda_b} \approx f^{(2)}_{\Lambda_b} \equiv f_{\Lambda_b} = 0.030 \pm 0.005$ GeV^3 [80]. The chiral-even (-odd) projector $M_{1(2)}$ reads

$$M_1(x_2,x_3) = \frac{\not{p}\not{n}}{4}\Psi_3^{+-}(x_2,x_3) + \frac{\not{n}\not{p}}{4}\Psi_3^{-+}(x_2,x_3),$$
$$M_2(x_2,x_3) = \frac{\not{n}}{\sqrt{2}}\Psi_2(x_2,x_3) + \frac{\not{p}}{\sqrt{2}}\Psi_4(x_2,x_3), \tag{7}$$

where two light-cone vectors $n = (1,0,\mathbf{0}_T)$ and $v = (0,1,\mathbf{0}_T)$ satisfy $n\cdot v = 1$. Here, n is parallel to the four-momentum p' of the Λ baryon in the massless limit. Several asymptotic models for the various twist LCDAs have been proposed in Refs. [57–59] and summarized in Refs. [55,81], which are also collected in Appendix A to make the paper self-contained.

The leading-twist Λ baryon LCDAs have been derived using QCD sum rules [61,82] and their higher-power corrections up to twist-6 were systematically presented in Refs. [83,84]. They involve 24 LCDAs with definite twists as well as ten independent nonperturbative parameters, which are needed to describe the local three-quark operator matrix elements. In order to reduce the nonperturbative parameters, we would like to adopt the LCDAs of the Λ baryon to the leading-twist accuracy in the present work. As will be shown in the next section, this scheme could yield satisfactory results with fewer parameters. The lattice QCD calculations of the leading-twist LCDAs of the full baryon octet have been performed; the reader is referred to Refs. [85–87] for details. In terms of the notation in Ref. [38], the nonlocal matrix element associated with the Λ baryon is decomposed into

$$(\Psi_\Lambda)_{\alpha\beta\gamma}(k_i',\mu) = \frac{1}{8\sqrt{2}N_c}\{(\not{p}'C)_{\beta\gamma}[\gamma_5\Lambda(p')]_\alpha\Phi^V(k_i',\mu) + (\not{p}'\gamma_5 C)_{\beta\gamma}[\Lambda(p')]_\alpha\Phi^A(k_i',\mu) + (i\sigma_{\mu\nu}p'^\nu C)_{\beta\gamma}[\gamma^\mu\gamma_5\Lambda(p')]_\alpha\Phi^T(k_i',\mu)\}, \tag{8}$$

with $\sigma_{\mu\nu} = i[\gamma_\mu,\gamma_\nu]/2$. The explicit forms of $\Phi^{V,A,T}$ at the scale $\mu = 1$ GeV have been studied using QCD sum rules [61,82]. In this work, we adopt the Chernyak-Ogloblin-Zhitnitsky (COZ) model proposed in Ref. [61]

$$\Phi^V(x_1,x_2,x_3) = 42 f_\Lambda \phi_{asy}[0.18(x_2^2-x_3^2) - 0.1(x_2-x_3)],$$
$$\Phi^A(x_1,x_2,x_3) = -42 f_\Lambda \phi_{asy}[0.26(x_3^2+x_2^2) + 0.34x_1^2 - 0.56x_2x_3 - 0.24x_1(x_2+x_3)],$$
$$\Phi^T(x_1,x_2,x_3) = 42 f_\Lambda^T \phi_{asy}[1.2(x_3^2-x_2^2) + 1.4(x_2-x_3)], \tag{9}$$

where $\phi_{asy}(x_1,x_2,x_3) = 120x_1x_2x_3$ denotes the asymptotic form in the limit of $\mu\to\infty$. The two normalization constants are fixed to be $f_\Lambda = 10 f_\Lambda^T = 6.3\times10^{-3}$ GeV^2 [61]. It is easy to observe that Φ^V and Φ^T are antisymmetric under permutation of two light quarks, but Φ^A is symmetric under the same operation. This is understandable because of the isospin symmetry of [ud] diquark in the Λ baryon. Φ^A and Φ^T satisfy the normalizations [61]

$$\int_0^1 \Phi^A dx_1dx_2dx_3\delta(1-x_1-x_2-x_3) = -f_\Lambda,$$
$$\int_0^1 \Phi^T x_2 dx_1dx_2dx_3\delta(1-x_1-x_2-x_3) = f_\Lambda^T, \tag{10}$$

where the δ function enforces momentum conservation.

The heavy-quarkonium production mechanism is still an open question. The nonrelativistic QCD (NRQCD) is one of the widely accepted theoretical frameworks to deal with the exclusive charmonium production processes, for which the amplitude can be factorized into the short-distance coefficients and the NRQCD long-distance matrix elements [88]. In NRQCD, a charmonium state could be produced through a $c\bar{c}$ pair in a color-octet state plus the emission of a soft gluon [89]. Although the color-octet matrix elements are suppressed by a factor of v^4 (the relative velocity between heavy quarks) in comparison to the color-singlet matrix elements, they are compensated by the associated larger short-distance coefficients. Particularly, the color-octet contributions to J/ψ production in the inclusive B decay were confirmed to be significant [89]. PQCD and NRQCD are very different approaches, which employ different expansion parameters. The DAs for the former are defined on the light cone and expanded in twist.

The matrix elements for the latter are defined in the nonrelativistic limit and expanded in v [90]. Therefore, the NRQCD matrix elements should not be employed in the PQCD approach. If the color-octet contributions are included in PQCD, the soft gluon from a DA is a physical parton and must attach to a hard kernel. They are the so-called three-parton DA contributions [91,92], which are of higher twist and suppressed by a power of $1/m_b$ with m_b being the b quark mass. As stated in [91], a three-parton contribution is about the order of magnitude of the higher Gegenbauer terms in the two-parton twist-3 DA, which is expected to be small. This smallness was also consistent with the observation made in the light-cone QCD sum rules [93]. Therefore, we only consider the contribution from the two-parton charmonium DAs within the accuracy of the current work, and the color-octet contribution through the three-parton DAs will be neglected due to its smallness.

The longitudinally and transversely polarized two-parton LCDAs up to twist-3 for charmonia are decomposed into [5]

$$\Psi_L = \frac{1}{\sqrt{2N_c}}(m\not{\epsilon}_L\psi^L + \not{\epsilon}_L\not{p}\psi^t),$$
$$\Psi_T = \frac{1}{\sqrt{2N_c}}(m\not{\epsilon}_T\psi^V + \not{\epsilon}_T\not{p}\psi^T), \tag{11}$$

where the expressions of various twists $\psi^{L,T,V,t}$ have been derived [62,63]

$$\psi^{L,T}(x,b) = \frac{f_\psi}{2\sqrt{2N_c}}N^{L,T}x\bar{x}\mathcal{T}(x,b) \times \exp\left\{-\frac{m_c}{\omega}x\bar{x}\left[\left(\frac{x-\bar{x}}{2x\bar{x}}\right)^2+\omega^2b^2\right]\right\},$$
$$\psi^{t}(x,b) = \frac{f_\psi}{2\sqrt{2N_c}}N^{t}(x-\bar{x})^2\mathcal{T}(x,b) \times \exp\left\{-\frac{m_c}{\omega}x\bar{x}\left[\left(\frac{x-\bar{x}}{2x\bar{x}}\right)^2+\omega^2b^2\right]\right\},$$
$$\psi^{V}(x,b) = \frac{f_\psi}{2\sqrt{2N_c}}N^{V}[1+(x-\bar{x})^2]\mathcal{T}(x,b) \times \exp\left\{-\frac{m_c}{\omega}x\bar{x}\left[\left(\frac{x-\bar{x}}{2x\bar{x}}\right)^2+\omega^2b^2\right]\right\}, \tag{12}$$

with m_c being the charm quark mass and $\bar{x} = 1-x$. We take the shape parameters $\omega = 0.6$ GeV for J/ψ [62] and $\omega = 0.2$ GeV for $\psi(2S)$ [63]. The normalization constants $N^{L,T,V,t}$ are related to the decay constants f_ψ via the normalization

$$\int_0^1 \psi^{L,T,V,t}(x,0)dx = \frac{f_\psi}{2\sqrt{2N_c}}. \tag{13}$$

The function $\mathcal{T}(x,b)$ reads [62,63]

$$\mathcal{T}(x,b) = \begin{cases} 1 & \text{for } J/\psi, \\ 1-4b^2m_c\omega x\bar{x}+\frac{m_c(x-\bar{x})^2}{\omega x\bar{x}} & \text{for } \psi(2S). \end{cases} \tag{14}$$

Based on the operator product expansion, the effective weak-interaction Hamiltonian for the $b \to sc\bar{c}$ transition reads [7]

$$\mathcal{H}_{\text{eff}} = \frac{G_F}{\sqrt{2}}\left\{V_{cb}V_{cs}^*[C_1(\mu)O_1(\mu)+C_2(\mu)O_2(\mu)] - \sum_{k=3}^{10}V_{tb}V_{ts}^*C_k(\mu)O_k(\mu)\right\} + \text{H.c.}, \tag{15}$$

where G_F is the Fermi constant, V_{ij} represent the Cabibbo-Kobayashi-Maskawa (CKM) matrix elements, $C_i(\mu)$ correspond to the Wilson coefficients evaluated at the renormalization scale μ, and O_i are the four-quark operators defined by

$$O_1 = \bar{c}_\alpha\gamma_\mu(1-\gamma_5)b_\beta \otimes \bar{s}_\beta\gamma^\mu(1-\gamma_5)c_\alpha,$$
$$O_2 = \bar{c}_\alpha\gamma_\mu(1-\gamma_5)b_\alpha \otimes \bar{s}_\beta\gamma^\mu(1-\gamma_5)c_\beta,$$
$$O_3 = \bar{s}_\beta\gamma_\mu(1-\gamma_5)b_\beta \otimes \sum_{q'}\bar{q}'_\alpha\gamma^\mu(1-\gamma_5)q'_\alpha,$$
$$O_4 = \bar{s}_\beta\gamma_\mu(1-\gamma_5)b_\alpha \otimes \sum_{q'}\bar{q}'_\alpha\gamma^\mu(1-\gamma_5)q'_\beta,$$
$$O_5 = \bar{s}_\beta\gamma_\mu(1-\gamma_5)b_\beta \otimes \sum_{q'}\bar{q}'_\alpha\gamma^\mu(1+\gamma_5)q'_\alpha,$$
$$O_6 = \bar{s}_\beta\gamma_\mu(1-\gamma_5)b_\alpha \otimes \sum_{q'}\bar{q}'_\alpha\gamma^\mu(1+\gamma_5)q'_\beta,$$
$$O_7 = \frac{3}{2}\bar{s}_\beta\gamma_\mu(1-\gamma_5)b_\beta \otimes \sum_{q'}e_{q'}\bar{q}'_\alpha\gamma^\mu(1+\gamma_5)q'_\alpha,$$
$$O_8 = \frac{3}{2}\bar{s}_\beta\gamma_\mu(1-\gamma_5)b_\alpha \otimes \sum_{q'}e_{q'}\bar{q}'_\alpha\gamma^\mu(1+\gamma_5)q'_\beta,$$
$$O_9 = \frac{3}{2}\bar{s}_\beta\gamma_\mu(1-\gamma_5)b_\beta \otimes \sum_{q'}e_{q'}\bar{q}'_\alpha\gamma^\mu(1-\gamma_5)q'_\alpha,$$
$$O_{10} = \frac{3}{2}\bar{s}_\beta\gamma_\mu(1-\gamma_5)b_\alpha \otimes \sum_{q'}e_{q'}\bar{q}'_\alpha\gamma^\mu(1-\gamma_5)q'_\beta. \tag{16}$$

The sum over q' runs over the quark fields that are active at the scale $\mu = \mathcal{O}(m_b)$. It is evident that the direct CP violations for the decay at hand are very small owing to an almost null weak phase from the CKM matrix element V_{ts}. The helicity amplitudes $H_{\lambda_\Lambda\lambda_\psi}$ are then given by sandwiching $\mathcal{H}_{\text{eff}}$ with the initial and final states,

$$H_{\lambda_\Lambda\lambda_\psi} = \langle\Lambda(\lambda_\Lambda)\psi(\lambda_\psi)|\mathcal{H}_{\text{eff}}|\Lambda_b(\lambda_{\Lambda_b})\rangle, \tag{17}$$

where λ_{Λ_b}, λ_Λ, and λ_ψ are the corresponding helicities. The helicity labels can take the values $\lambda_\Lambda = \pm 1/2$ and

$\lambda_\psi = 0, \pm 1$. Angular momentum conservation in the Λ_b decay requires $|\lambda_\Lambda - \lambda_\psi| = 1/2$. Thereby, the decay can be described by four independent complex helicity amplitudes, namely, $H_{-\frac{1}{2}-1}$, $H_{\frac{1}{2}1}$, $H_{\frac{1}{2}0}$, and $H_{-\frac{1}{2}0}$, in the helicity-based definition. The former two terms correspond to the transverse polarizations for the charmonium and the last two terms to the longitudinal ones. As we will see later, the helicity amplitudes are particularly convenient for expressing various observable quantities in the decays.

In general, it is convenient to analyze the decay in terms of the invariant amplitudes, which can be expanded with the Dirac spinors and polarization vector as

$$\begin{aligned}\mathcal{M}^L &= \bar{u}_\Lambda(p')\epsilon_L^{\mu*}\left[A_1^L\gamma_\mu\gamma_5 + A_2^L\frac{p'_\mu}{M}\gamma_5 + B_1^L\gamma_\mu + B_2^L\frac{p'_\mu}{M}\right] \\ &\quad \times u_{\Lambda_b}(p), \\ \mathcal{M}^T &= \bar{u}_\Lambda(p')\epsilon_T^{\mu*}[A_1^T\gamma_\mu\gamma_5 + B_1^T\gamma_\mu]u_{\Lambda_b}(p), \end{aligned} \tag{18}$$

where $A_{1,2}^{L,T}$ and $B_{1,2}^{L,T}$ are the so-called invariant amplitudes with L and T in the superscripts denoting the longitudinal and transverse components, respectively. We emphasize that the two structures $A_1^L\gamma_\mu\gamma_5$ and $A_2^L\frac{p'_\mu}{M}\gamma_5$ appearing in the above equations are not independent. The same statement is also true for the $B_1^L\gamma_\mu$ and $B_2^L\frac{p'_\mu}{M}$ terms. It is easy to prove it by expressing the longitudinal polarization vector in terms of momenta p and p', and using the equations of motion for the two spinors. In fact, there are also four independent invariant amplitudes, as there should be. The explicit relations between the helicity amplitudes $H_{\lambda_\Lambda\lambda_\psi}$ and the invariant amplitudes A, B are [32,94].

$$\begin{aligned} H_{\frac{1}{2}1} &= -(\sqrt{Q_+}A_1^T + \sqrt{Q_-}B_1^T), \\ H_{-\frac{1}{2}-1} &= \sqrt{Q_+}A_1^T - \sqrt{Q_-}B_1^T, \\ H_{\frac{1}{2}0} &= \frac{1}{\sqrt{2}m}[\sqrt{Q_+}(M - m_\Lambda)A_1^L - \sqrt{Q_-}P_cA_2^L \\ &\quad + \sqrt{Q_-}(M + m_\Lambda)B_1^L + \sqrt{Q_+}P_cB_2^L], \\ H_{-\frac{1}{2}0} &= \frac{1}{\sqrt{2}m}[-\sqrt{Q_+}(M - m_\Lambda)A_1^L + \sqrt{Q_-}P_cA_2^L \\ &\quad + \sqrt{Q_-}(M + m_\Lambda)B_1^L + \sqrt{Q_+}P_cB_2^L], \end{aligned} \tag{19}$$

with $Q_\pm = (M \pm m_\Lambda)^2 - m^2$. P_c denotes the modulus of the three momentum of the Λ in the Λ_b rest frame.

The general factorization formula for any one of the invariant amplitudes in Eq. (18) can be written as

$$\begin{aligned}\mathcal{F} &= \frac{f_{\Lambda_b}\pi^2 G_F}{18\sqrt{3}}\sum_{ij}\int [\mathcal{D}x][\mathcal{D}b]_{T_{ij}}\alpha_s^2(t_{T_{ij}})\Omega_{T_{ij}}(b, b', b_q) \\ &\quad \times e^{-S_{T_{ij}}}[V^{LL}H_{T_{ij}}^{LL}(x, x', y) + V^{SP}H_{T_{ij}}^{SP}(x, x', y)], \end{aligned} \tag{20}$$

where the summation extends over all possible diagrams as shown in Fig. 1. V denotes the product of the CKM matrix elements and the Wilson coefficients, where the superscripts LL and SP correspond to the contributions from the (V-A)(V-A) and (S-P)(S + P) operators, respectively. $H_{T_{ij}}$ is the numerator of the hard amplitude depending on the spin structure of the final state. These quantities associated with specific diagram are collected in Appendix B. $\Omega_{T_{ij}}$ is the Fourier transformation of the denominator of the hard amplitude from the k_T space to its conjugate b space. Their explicit formulas can be found in Ref. [56] and shall not be repeated here. The integration measure of the momentum fractions are defined as

$$\begin{aligned}[\mathcal{D}x] &= [dx][dx']dy, \\ [dx] &= dx_1dx_2dx_3\delta(1 - x_1 - x_2 - x_3), \\ [dx'] &= dx'_1dx'_2dx'_3\delta(1 - x'_1 - x'_2 - x'_3), \end{aligned} \tag{21}$$

and the measure of the transverse extents $[\mathcal{D}b]$ are also shown in Ref. [56].

The Sudakov factors in Eq. (20) coming from the k_T resummation are given by [54]

$$\begin{aligned}S_{T_{ij}} &= \sum_{l=2,3}s(w, k_l^-) + \sum_{l=1,2,3}s(w', k_l'^+) + \frac{8}{3}\int_{\kappa w}^{t_{T_{ij}}}\frac{d\bar{\mu}}{\bar{\mu}}\gamma_q(\alpha_s(\bar{\mu})) \\ &\quad + 3\int_{\kappa w'}^{t_{T_{ij}}}\frac{d\bar{\mu}}{\bar{\mu}}\gamma_q(\alpha_s(\bar{\mu})), \end{aligned} \tag{22}$$

$$\begin{aligned}S_{T_{ij}} &= \sum_{l=2,3}s(w, k_l^-) + \sum_{l=1,2,3}s(w', k_l'^+) + \sum_{l=1,2}s_c(w_q, q_l^-) \\ &\quad + \frac{8}{3}\int_{\kappa w}^{t_{T_{ij}}}\frac{d\bar{\mu}}{\bar{\mu}}\gamma_q(\alpha_s(\bar{\mu})) + 3\int_{\kappa w'}^{t_{T_{ij}}}\frac{d\bar{\mu}}{\bar{\mu}}\gamma_q(\alpha_s(\bar{\mu})) \\ &\quad + 2\int_{\kappa w_q}^{t_{T_{ij}}}\frac{d\bar{\mu}}{\bar{\mu}}\gamma_q(\alpha_s(\bar{\mu})) \end{aligned} \tag{23}$$

for the factorizable and nonfactorizable diagrams, respectively. The explicit expressions of the function $s_{(c)}$ can be found in Refs. [73,95]. Another threshold Sudakov factor $S_t(x)$ collecting the double logarithms $\alpha_s\ln^2(x)$ to all orders is set to 1, similar to the case of the $\Lambda_b \to p$ decays [55]. The phenomenological factor $\kappa = 1.14$ is adopted according to Ref. [96].

The hard scale t for each diagram is chosen as the maximal virtuality of internal particles including the factorization scales in a hard amplitude:

$$t_{T_{ij}} = \max(\sqrt{|t_A|}, \sqrt{|t_B|}, \sqrt{|t_C|}, \sqrt{|t_D|}, w, w', w_q), \tag{24}$$

where the expressions of $t_{A,B,C,D}$ are listed in Appendix B. The factorization scales w, w', and w_q are defined by

$$w^{(\prime)} = \min\left(\frac{1}{b_1^{(\prime)}}, \frac{1}{b_2^{(\prime)}}, \frac{1}{b_3^{(\prime)}}\right), \qquad w_q = \frac{1}{b_q}, \tag{25}$$

with the variables

$$b_1^{(\prime)} = |b_2^{(\prime)} - b_3^{(\prime)}|, \tag{26}$$

and the other $b_l^{(\prime)}$ defined by permutation.

III. NUMERICAL RESULTS

We first present all the pertinent inputs for our numerical calculations. Various masses (GeV), lifetimes (ps), and the Wolfenstein parameters for the CKM matrix are summarized below [18]

$$\begin{aligned} &M = 5.6196, \quad m_\Lambda = 1.116, \quad m_b = 4.8, \\ &m_c = 1.275, \quad m_{J/\psi} = 3.097, \quad m_{\psi(2S)} = 3.686, \\ &\tau = 1.464, \quad \lambda = 0.22650, \quad A = 0.790, \\ &\bar{\rho} = 0.141, \quad \bar{\eta} = 0.357. \end{aligned} \tag{27}$$

The decay constant of J/ψ has been studied using the lattice QCD method [97], while the $\psi(2S)$ one is still not available. Here we choose $f_{J/\psi} = 0.363^{+0.089}_{-0.088}$ GeV and $f_{\psi(2S)} = 0.309 \pm 0.076$ GeV obtained from the calculation of the S-wave quarkonium wave functions at the origin in the $\overline{\rm MS}$ scheme based on nonrelativistic effective field theories [98]. Other nonperturbative parameters appearing in the hadron LCDAs have been specified before.

The calculations of the $\Lambda_b \to \Lambda$ transition form factors are similar to that of $\Lambda_b \to \Lambda_c$ [56], the matrix of which is induced by the $V - A$ current has the general form

$$\begin{aligned} \langle \Lambda(p')|\bar{s}\gamma^\mu b|\Lambda_b(p)\rangle &= \bar{u}_\Lambda(p')[f_1(q^2)\gamma^\mu - \frac{f_2(q^2)}{M} i\sigma^{\mu\nu}q_\nu \\ &\quad + \frac{f_3(q^2)}{M} q^\mu] u_{\Lambda_b}(p), \\ \langle \Lambda(p')|\bar{s}\gamma^\mu\gamma_5 b|\Lambda_b(p)\rangle &= \bar{u}_\Lambda(p')[g_1(q^2)\gamma^\mu - \frac{g_2(q^2)}{M} i\sigma^{\mu\nu}q_\nu \\ &\quad + \frac{g_3(q^2)}{M} q^\mu]\gamma_5 u_{\Lambda_b}(p), \end{aligned} \tag{28}$$

where $q = p - p'$ denotes the transferred momentum between the initial and final baryons. Here, we shall concentrate on f_1 and g_1, which can be extracted from the factorizable decay amplitudes [56]. We first compare the results at zero momentum transfer ($q^2 = 0$) from various models for the Λ_b baryon LCDAs in Table I. The values from the first five models are found to be of similar size, but the numbers in the last column, which correspond to the Gaussian-type model, are at least an order of magnitude lower. This is ascribed to the Gaussian-type model yielding a severe suppression at the end point region $x_1 \sim 1$, where the b quark carries most of the Λ_b baryon momentum. On the contrary, other models have a strong peak in that region as shown in the Fig. 2 of Ref. [55]. The different behaviors at the end point region cause the results derived from the Gaussian-type model to be generally smaller. Actually, a similar case also occurred in earlier PQCD calculations [50,54] on the $\Lambda_b \to p$ transition form factors with the Gaussian-type Λ_b LCDAs, which are also quite small, at the level of 10^{-3}. A recent reanalysis in PQCD [55] found that the values increased significantly by using other models instead of the Gaussian-type one.

We also examine the effect of different Λ baryon LCDAs on the numerical results. As aforementioned, there are two alternative models for the Λ baryon LCDAs: one from the light-cone QCD sum rules (QCDSR) [83] including the higher-power corrections up to twist-6 and the other from the lattice QCD [85,87] with leading-twist accuracy. Using the inputs in Ref. [83], we obtain the form factors with only the twist-3 contributions $f_1(0) = 2.1$ and $g_1(0) = 1.8$, which were incredibly large. The reason is that the coefficient of the linear term of Eq. (46) in Ref. [83] is 2 orders of magnitude greater than the analogous term in Eq. (9). Taking into account contributions up to twist-6 LCDAs, the corresponding values above become -5.2 and -0.08, respectively, which seems to contradict with the heavy-quark symmetry. As stressed in Refs. [85,87], the shape parameters from the lattice QCD calculations are generally several factors below the COZ estimates in Ref. [61], resulting in much smaller form factors when utilizing the lattice QCD parameters. The values may be enhanced by including contributions from higher twist LCDAs but which are currently unavailable in lattice QCD. Hence, to obtain a reasonable estimate under the PQCD framework, we will employ the exponential model [59] for the Λ_b baryon LCDAs and the leading-twist Λ baryon LCDAs with the corresponding parameters from the COZ model [61] in the subsequent analysis.

TABLE I. PQCD predictions for the form factors f_1 and g_1 at $q^2 = 0$ of the $\Lambda_b \to \Lambda$ transition with the various models of the Λ_b LCDAs.

Form factors	Exponential model	Free-parton approximation	Gegenbauer-1	Gegenbauer-2	QCDSR model	Gaussian-type
$f_1(0)$	0.095	0.125	0.090	0.093	0.122	0.004
$g_1(0)$	0.104	0.136	0.102	0.104	0.129	0.005

TABLE II. Theoretical predictions for the form factors f_1 and g_1 at $q^2 = 0$ of the $\Lambda_b \to \Lambda$ transition.

Form factors	This work	[35]	[44,101]	[102]	[60]	[103]	[99]	[100]	[36]	[39]	[47]	[32]
$f_1(0)$	$0.095^{+0.057+0.018}_{-0.029-0.021}$	0.1081	0.107	0.061	0.18 ± 0.04	~ 0.20	0.322 ± 0.112	0.446	0.025	$0.131^{+0.016+0.008}_{-0.018-0.008}$	0.175 ± 0.106	0.062
$g_1(0)$	$0.104^{+0.060+0.016}_{-0.033-0.020}$	0.1065	0.104	0.107	⋯	⋯	0.318 ± 0.110	0.446	0.028	$0.132^{+0.016+0.008}_{-0.017-0.009}$	⋯	0.108

In Table II, we compare our results on the form factors at $q^2 = 0$ to those obtained in other works, where the first and second uncertainties arise from the shape parameter $\omega_0 = 0.4 \pm 0.1$ in the Λ_b baryon LCDAs for the exponential model and hard scale t varying from $0.75t$ to $1.25t$, respectively. It is found that the predominant uncertainties in our calculations stem from the baryon LCDAs, which can reach 50% in magnitude. The relevant nonperturbative parameters in the LCDAs also need to be constrained to further improve the precision of theoretical predictions. Broadly, our results agree reasonably well with the results from the light-front quark model [35], covariant confined quark model (CCQM) [44], and the covariant light-front quark model [39] with the diquark approximation. The values from the QCDSR [99] and Heavy Quark Effective Theory (HQET) [100] are several times larger but still at the same order. However, the numbers from the nonrelativistic quark model [36] are quite small, at the order of 10^{-2}. Despite a wide range of various predictions, the nearly equal relation $f_1(0) \sim g_1(0)$ holds for the most approaches, which is expected in the heavy-quark limit.

Next, we turn to the decay amplitudes of the concerned decays. The factorizable and nonfactorizable contributions to the invariant amplitudes are presented in Table III. Note that the imaginary parts of the factorizable amplitudes arise due to the vertex corrections. The decay amplitudes are clearly governed by the imaginary part of the nonfactorizable contributions. The factorizable contributions are smaller by 1 or 2 orders of magnitude, despite receiving the enhancement from the vertex corrections. Previous PQCD investigations [38] have also observed a similar feature. This situation differs from the case of color-suppressed decays in the B meson sector, where factorizable diagram contributions could be comparable to nonfactorizable ones after including the vertex corrections [66,104].

Following Ref. [48], we introduce the moduli squared of normalized helicity amplitudes $|\hat{H}_{\lambda_\Lambda \lambda_\psi}|^2 = |H_{\lambda_\Lambda \lambda_\psi}|^2 / H_N$ with

$$H_N = |H_{\frac{1}{2}1}|^2 + |H_{-\frac{1}{2}-1}|^2 + |H_{\frac{1}{2}0}|^2 + |H_{-\frac{1}{2}0}|^2. \quad (29)$$

The calculation of the normalized squared helicity amplitudes can be done in a straightforward way by combining Eqs. (19) and (29) and Table III, whose numerical results are exhibited in Table IV. The values given in the parentheses are the corresponding phases. The sources of the errors in the numerical estimates have the same origin as in the discussion of the form factors in Table II. Note that these quantities are less sensitive to the considered uncertainties since the errors partially cancel in the ratios; thus, we have added them in quadrature. It is observed that the considered decays receive significant contributions from $H_{-\frac{1}{2}-1}$ and $H_{-\frac{1}{2}0}$, which means the negative-helicity states for the Λ baryon are preferred. Contributions from the $\lambda_\Lambda = \frac{1}{2}$ helicity states are rather small, which amounts to less than 10%. This pattern is consistent with the expectation from the heavy-quark limit and the left-handed nature of the weak interaction [23]. Experimentally, a fit to the

TABLE III. The values of the invariant amplitudes from the factorizable and nonfactorizable diagrams for $\Lambda_b \to \Lambda\psi$ decays. Only central values are presented here.

Amplitude	Factorizable	Nonfactorizable
$A_1^L(\Lambda_b \to \Lambda J/\psi)$	$3.57 \times 10^{-11} + i3.55 \times 10^{-10}$	$8.12 \times 10^{-9} - i2.50 \times 10^{-8}$
$B_1^L(\Lambda_b \to \Lambda J/\psi)$	$-6.06 \times 10^{-11} - i4.17 \times 10^{-10}$	$-6.87 \times 10^{-9} + i2.28 \times 10^{-8}$
$A_2^L(\Lambda_b \to \Lambda J/\psi)$	$-1.32 \times 10^{-11} - i8.66 \times 10^{-11}$	$2.22 \times 10^{-10} + i7.35 \times 10^{-9}$
$B_2^L(\Lambda_b \to \Lambda J/\psi)$	$1.81 \times 10^{-11} + i1.30 \times 10^{-10}$	$8.08 \times 10^{-9} - i8.59 \times 10^{-9}$
$A_1^T(\Lambda_b \to \Lambda J/\psi)$	$5.79 \times 10^{-11} + i3.29 \times 10^{-10}$	$7.41 \times 10^{-9} - i2.95 \times 10^{-8}$
$B_1^T(\Lambda_b \to \Lambda J/\psi)$	$-8.42 \times 10^{-11} - i3.91 \times 10^{-10}$	$-6.82 \times 10^{-9} + i2.90 \times 10^{-8}$
$A_1^L(\Lambda_b \to \Lambda\psi(2S))$	$1.01 \times 10^{-10} + i5.14 \times 10^{-10}$	$8.69 \times 10^{-9} - i2.85 \times 10^{-8}$
$B_1^L(\Lambda_b \to \Lambda\psi(2S))$	$-1.60 \times 10^{-10} - i6.15 \times 10^{-10}$	$-8.57 \times 10^{-9} + i2.68 \times 10^{-8}$
$A_2^L(\Lambda_b \to \Lambda\psi(2S))$	$-3.45 \times 10^{-11} - i1.43 \times 10^{-10}$	$3.04 \times 10^{-9} + i1.63 \times 10^{-8}$
$B_2^L(\Lambda_b \to \Lambda\psi(2S))$	$5.35 \times 10^{-11} + i2.25 \times 10^{-10}$	$9.12 \times 10^{-9} - i1.06 \times 10^{-8}$
$A_1^T(\Lambda_b \to \Lambda\psi(2S))$	$1.41 \times 10^{-10} + i4.60 \times 10^{-10}$	$6.90 \times 10^{-9} - i2.25 \times 10^{-8}$
$B_1^T(\Lambda_b \to \Lambda\psi(2S))$	$-2.01 \times 10^{-10} - i5.53 \times 10^{-10}$	$-6.83 \times 10^{-9} + i2.24 \times 10^{-8}$

angular distribution of the cascade decay $\Lambda_b \to \Lambda(p\pi^-)J/\psi(\mu^+\mu^-)$ has been performed by the LHCb [19], ATLAS [20], and CMS [21,22] Collaborations, which allows us to determine the helicity amplitudes from the fitted angular parameters. The measured results together with the predictions from the CCQM [44,48] are also presented in Table IV for comparison. Our results are comparable with CCQM calculations and experiments. We note that some determined helicity amplitudes squared from the LHCb and CMS experiments are negative and therefore nonphysical. This is because they use an old average value of $\alpha_\Lambda = 0.642 \pm 0.013$ from Refs. [105–109], which is smaller than the recent measurements by the BES III [110] and LHCb [23] Collaborations and an independent estimate of kaon photoproduction scattering data by CLAS Collaboration in Ref. [111].

The only available experimental information about the phase of the helicity amplitudes for the $\Lambda_b \to \Lambda J/\psi$ decay comes from the recent measurements by LHCb [23]. The phase of b_+, which corresponds to our $\arg(\hat{H}_{-\frac{1}{2}-1})$, is fixed to be zero, while the phases of the remaining three helicity amplitudes are measured relative to $\arg(b_+)$. Following the definition given in Ref. [23], one can estimate the three relative phases (in rad) from Table IV to be

$$\begin{aligned}
\arg(a_+) &= 0.22^{+0.00}_{-0.38}(0.01^{+0.06}_{-0.05}),\\
\arg(a_-) &= -3.13^{+0.00}_{-0.07}(3.09^{+0.10}_{-0.01}),\\
\arg(b_-) &= -3.12^{+0.03}_{-0.08}(3.14^{+0.05}_{-0.02}),
\end{aligned} \tag{30}$$

where the corresponding numbers for the $\psi(2S)$ mode are shown in parentheses. Because the imaginary part of the amplitude contributes significantly more than the real part as mentioned before, these amplitude vectors are scattered toward the imaginary axis of the complex plane, resulting in phase differences that either approach zero or $\pm\pi$. Although our central values are away from the most probable values from the LHCb experiment, they still fall into the 95% credibility intervals. Since the measured phases span wide intervals, we cannot draw anymore definite conclusions. A measurement with improved precision on the phases would be highly desirable.

Armed with the helicity amplitudes derived above, we can now proceed to perform the calculations of the decay branching ratios and various asymmetry parameters, which are defined as [19,48]

$$\begin{aligned}
\mathcal{B} &= \frac{P_c \tau_{\Lambda_b}}{8\pi M^2} H_N,\\
\alpha_b &= -|\hat{H}_{\frac{1}{2}1}|^2 + |\hat{H}_{-\frac{1}{2}-1}|^2 + |\hat{H}_{\frac{1}{2}0}|^2 - |\hat{H}_{-\frac{1}{2}0}|^2,\\
\alpha_2 &= |\hat{H}_{\frac{1}{2}1}|^2 - |\hat{H}_{-\frac{1}{2}-1}|^2 + |\hat{H}_{\frac{1}{2}0}|^2 - |\hat{H}_{-\frac{1}{2}0}|^2,\\
r_0 &= |\hat{H}_{\frac{1}{2}1}|^2 + |\hat{H}_{-\frac{1}{2}0}|^2,\\
r_1 &= |\hat{H}_{\frac{1}{2}1}|^2 - |\hat{H}_{-\frac{1}{2}0}|^2,
\end{aligned} \tag{31}$$

where α_b is the parity-violating asymmetry parameter, α_2 represents the longitudinal polarization of the daughter Λ baryon, and $r_0(r_1)$ corresponds to the longitudinal unpolarized (polarized) parameter. The numerical results are collected in Table V in comparison with CCQM calculations and available experimental data [43,44,48]. Some important features of the numerical results are the following:

(1) The obtained branching ratios for the two modes are both of order 10^{-4}. As aforementioned, there is no experimental data on the absolute branching ratios due to the fact that the fragmentation fraction of the b quark to Λ_b baryon are not well determined yet. Using the estimates of the fragmentation fraction $f(b \to \Lambda_b) = (7\text{–}17.5)\%$ from Refs. [47,112,113], we can convert the data in Eq. (1) into the possible range $\mathcal{B}(\Lambda_b \to \Lambda J/\psi) \sim (3.3\text{–}8.3) \times 10^{-4}$, which overlaps our central value in Table V. Likewise, no absolute measurement of the decay rate for the

TABLE IV. The magnitude squared of normalized helicity amplitudes for the $\Lambda_b \to \Lambda\psi$ decays, where the numbers in parenthesises are the corresponding phases defined in the range $[-\pi, \pi]$ rad. The sources of the theoretical errors are the same as in Table II but added in quadrature. For comparison, the experimental data [19,20,22] as well as the available predictions from CCQM [44,48] are also presented. The superscript "2" for the ATLAS results means square.

Mode	$\lvert\hat{H}_{\frac{1}{2}1}\rvert^2$	$\lvert\hat{H}_{-\frac{1}{2}-1}\rvert^2$	$\lvert\hat{H}_{\frac{1}{2}0}\rvert^2$	$\lvert\hat{H}_{-\frac{1}{2}0}\rvert^2$
$\Lambda_b \to \Lambda J/\psi$				
This work	$0.044^{+0.010}_{-0.007}(1.84^{+0.06}_{-0.09})$	$0.484^{+0.041}_{-0.035}(-1.32^{+0.04}_{-0.01})$	$0.037^{+0.014}_{-0.003}(-1.11^{+0.00}_{-0.36})$	$0.435^{+0.041}_{-0.063}(1.82^{+0.01}_{-0.05})$
CCQM [48]	2.34×10^{-3}	0.465	3.24×10^{-4}	0.532
CCQM [44]	3.1×10^{-3}	0.47	4.6×10^{-4}	0.53
LHCb [19]	$-0.10 \pm 0.04 \pm 0.03$	$0.51 \pm 0.05 \pm 0.02$	$0.01 \pm 0.04 \pm 0.03$	$0.57 \pm 0.06 \pm 0.03$
ATLAS [20]	$(0.08^{+0.13}_{-0.08} \pm 0.06)^2$	$(0.79^{+0.04}_{-0.05} \pm 0.02)^2$	$(0.17^{+0.12}_{-0.17} \pm 0.09)^2$	$(0.59^{+0.06}_{-0.07} \pm 0.03)^2$
CMS [22]	$0.05 \pm 0.04 \pm 0.04$	$0.52 \pm 0.04 \pm 0.04$	$-0.10 \pm 0.04 \pm 0.04$	$0.51 \pm 0.03 \pm 0.04$
$\Lambda_b \to \Lambda\psi(2S)$				
This work	$0.051^{+0.003}_{-0.004}(1.88^{+0.04}_{-0.05})$	$0.365^{+0.028}_{-0.020}(-1.26^{+0.02}_{-0.05})$	$0.061^{+0.003}_{-0.011}(-1.25^{+0.03}_{-0.09})$	$0.523^{+0.035}_{-0.030}(1.83^{+0.06}_{-0.00})$
CCQM [44]	1.2×10^{-2}	0.54	3.3×10^{-3}	0.45

TABLE V. Branching ratios (10^{-4}) and asymmetry paramaters for the $\Lambda_b \to \Lambda\psi$ decays. The sources of our theoretical errors are the same as in Table II.

Mode	$\mathcal{B}$	α_b	α_2	r_0	r_1
$\Lambda_b \to \Lambda J/\psi$					
This work	$7.75^{+4.08+1.39}_{-3.17-0.96}$	$0.042^{+0.104+0.027}_{-0.069-0.001}$	$-0.84^{+0.05+0.01}_{-0.01-0.00}$	$0.47^{+0.04+0.00}_{-0.05-0.02}$	$-0.40^{+0.07+0.01}_{-0.04-0.00}$
CCQM [43,48]	8.0	−0.069	−0.995	0.533	−0.532
LHCb [19]	⋯	$0.05 \pm 0.17 \pm 0.17$	⋯	$0.58 \pm 0.02 \pm 0.01$	$-0.56 \pm 0.10 \pm 0.05$
ATLAS [20]	⋯	$0.30 \pm 0.16 \pm 0.16$	⋯	⋯	⋯
CMS [22]	⋯	$-0.14 \pm 0.14 \pm 0.10$	$-1.11 \pm 0.04 \pm 0.05$	⋯	⋯
$\Lambda_b \to \Lambda\psi(2S)$					
This work	$3.63^{+1.91+0.70}_{-1.39-0.41}$	$-0.149^{+0.033+0.044}_{-0.048-0.040}$	$-0.78^{+0.00+0.01}_{-0.02-0.02}$	$0.58^{+0.02+0.02}_{-0.02-0.02}$	$-0.46^{+0.02+0.03}_{-0.04-0.03}$
CCQM [44]	7.25	0.09	−0.97	0.45	−0.44

$\psi(2S)$ decay is provided, but its relative rate with respect to the J/ψ one has been measured by the ATLAS [28] and LHCb [29] Collaborations. The ratio in PQCD is estimated to be $\mathcal{R} = \frac{\mathcal{B}(\Lambda_b \to \Lambda\psi(2S))}{\mathcal{B}(\Lambda_b \to \Lambda J/\psi)} = 0.47^{+0.02}_{-0.00}$, where all uncertainties are added in quadrature. It is apparent that this ratio is less sensitive to the variations of hadronic parameters involved in the baryon LCDAs than the individual branching ratios, since the parameter dependence of the PQCD predictions for the branching ratios are largely canceled in their relative ratios. Our prediction is consistent with the PDG average value of $\mathcal{R} = 0.508 \pm 0.023$ [18] within uncertainties. Although the predicted branching ratio $\mathcal{B}(\Lambda_b \to \Lambda J/\psi))$ from CCQM agrees well with our result, its value for the $\psi(2S)$ mode one is twice larger, leading to a larger value $\mathcal{R} = 0.8 \pm 0.1$ [44,45]. In addition, Wei *et al.* [35] used the light-front quark model by treating the spectator quarks as a diquark system and found $\mathcal{R} = 0.65$. Mott and Roberts [36] also studied the same topic in a nonrelativistic quark model. They estimated the ratio even exceeding 1, which seems to be unexpected since the decay process involving the radial excited states in the final state usually has a lower rate. This demonstrates that the currently available theoretical calculations of the ratio are generally greater than our result as well as the data.

(2) It is observed from Table V that the predicted up-down asymmetries for the two modes seem to be distinctly different. For the J/ψ mode, we obtained the small positive central value $\alpha_b = 0.042$, while that of the $\psi(2S)$ mode is larger in size but with a minus sign. According to the definition of the α_b in Eq. (31), its value is sensitive to the difference of two dominant helicity amplitudes $|\hat{H}_{-\frac{1}{2}-1}|$ and $|\hat{H}_{-\frac{1}{2}0}|$. As can be seen from Table III, the transverse components are reduced going from the J/ψ mode to the $\psi(2S)$ mode, but the longitudinal ones are the opposite. It is understandable since the dominant nonfactorizable contributions are process dependent. A negative up-down asymmetry appears when the longitudinal polarization amplitude exceeds the transverse one. The previous measurements of α_b by LHCb [19], ATLAS [20], and CMS [22] for the J/ψ channel have large errors. The central values given by LHCb [19] and ATLAS [20] are both positive, while CMS [22] reports a negative one as shown in Table V. Measurements that are more precise have been released recently by LHCb [23] using data collected with the LHCb experiment during Runs 1 and 2 of the LHC. The resulting most probable value of α_b is −0.022 with a 68% credibility interval from −0.048 to 0.005, which covers our calculation with error bars.

(3) The Λ longitudinal polarizations α_2 are significantly smaller than those calculations from CCQM [43,44,48]. From Table IV, one can see the contributions from the positive-helicity states in CCQM are strongly suppressed at the level of 10^{-3}. Nonetheless, the corresponding quantities in PQCD have a order of 10^{-2} due to the inclusion of the nonfactorizable contributions. The CCQM calculations are based on the factorization approximation, in which the hadronic matrix element for a two-body baryon decay process is factorized into a product of a baryonic transition form factor and the meson decay constant. The nonfactorizable effects enter into the effective Wilson coefficients in the scenario of the effective color number, which can be totally factorized out within the factorization framework and canceled in the longitudinal polarizations α_2. In contrast, the nonfactorizable contributions in the PQCD calculations are related to the decay processes and are also helicity dependent [5]. In the absence of the nonfactorizable contributions, the PQCD predictions of the Λ longitudinal polarizations for the J/ψ and $\psi(2S)$ modes will be increased to −0.94 and −0.90, respectively, which are closer to the CCQM results. As a by-product, the obtained value of α_2 allows us to estimate the forward-backward (FB) asymmetry with respect to the

TABLE VI. Various predictions in the literature of the $\Lambda_b \to \Lambda J/\psi$ decay, where the branching ratio is in units of 10^{-4}.

	[31]	[32]	[33]	[34,40]	[35]	[36]	[37][a]	[38]	[39]	[41]	[42,47]	[46,114][b]
$\mathcal{B}$	2.49	1.6	6.04	2.7	3.94	8.2	5.0–7.8	1.65–5.27	$3.33^{+0.48+0.56+0.32}_{-0.20-0.63-0.30}$	2.1	3.3 ± 2.0	12.5/4.4/1.2
α_b	−0.208	−0.10	−0.18	−0.21	−0.204	−0.09	⋯	−0.17 to −0.14	-0.21 ± 0.00	−0.11	⋯	0.777

[a]We quote the values in the large N_c limit.
[b]The quoted values correspond to $N_c^{\rm eff} = 2$, 2.5, and 3, respectively.

hadron-side polar angle [44] $\mathcal{A}_{FB} \equiv \alpha_2\alpha_\Lambda = -0.613^{+0.045}_{-0.022}(-0.568^{+0.016}_{-0.033})$, where the number in parentheses is the corresponding value for the $\psi(2S)$ mode. In the estimates, we have used the new experimental PDG average value for the asymmetry parameter $\alpha_\Lambda = 0.732 \pm 0.014$ [18]. The PQCD predictions of the FB asymmetry above can be confronted with data in the future.

(4) The predicted longitudinal unpolarized r_0 and polarized r_1 are comparable with the CCQM calculations [43,48] and the reported values by the LHCb Collaboration [19] within errors.

(5) There is another interesting parameter γ_0 defined via [44]

$$\gamma_0 = |\hat{H}_{\frac{1}{2}1}|^2 + |\hat{H}_{-\frac{1}{2}-1}|^2 - 2|\hat{H}_{\frac{1}{2}0}|^2 - 2|\hat{H}_{-\frac{1}{2}0}|^2, \quad (32)$$

which denotes the longitudinal/transverse composition of the charmonium meson. The exact numbers in PQCD are $-0.416^{+0.089}_{-0.064}$ and $-0.753^{+0.056}_{-0.044}$ for the J/ψ and $\psi(2S)$ modes, respectively. The former differs by 1.6σ from the CMS measurement $-0.27 \pm 0.08 \pm 0.11$ [22] but matches its previous value $-0.46 \pm 0.07 \pm 0.04$ [21] within 1.0σ. A measurement with improved precision helps to better understand this possible discrepancy.

As previously stated, many other studies have been conducted of the $\Lambda_b \to \Lambda J/\psi$ decay but have primarily focused on the decay branching ratio and the up-down asymmetry. For the sake of comparison, we briefly summarize the currently available theoretical results in Table VI. Most of the various approaches give predictions of the same order of magnitude for the decay branching ratio. Our results coincide with those of the quark model in the large N_c limit [37] and the nonrelativistic quark model [36] but generally higher than other predictions. On the other hand, our prediction of the up-down asymmetry for the J/ψ mode is small in size with positive central value. A variety of quark-model-based analyses and predictions gave negative values ranging from −0.09 to −0.21, whereas the calculation of HQET provided a sizable positive value of 0.77 [46,114]. Hence, an accurate measurement of the branching ratio and up-down asymmetry parameter will enable us to discern different model predictions. We mention that our branching ratio and the up-down asymmetry for the J/ψ mode differ from those of the previous PQCD calculations [38] mainly because we updated the nonperturbation hadron LCDAs as discussed at length in the previous section.

Finally, we discuss the long-distance (LD) effects on the decay rate for the semileptonic $\Lambda_b \to \Lambda l^+ l^-$ decays with $l = e$, μ, τ in the vicinity of the charmonium resonance regions defined by [115]

$$\begin{aligned}\mathcal{B}_{\rm LD}(\Lambda_b \to \Lambda l^+ l^-) = {} & \mathcal{B}(\Lambda_b \to \Lambda J/\psi) \times \mathcal{B}(J/\psi \to l^+ l^-) \\ & + \mathcal{B}(\Lambda_b \to \Lambda\psi(2S)) \\ & \times \mathcal{B}(\psi(2S) \to l^+ l^-), \end{aligned} \quad (33)$$

where other higher radial excitations are not included here since their dileptonic decay rates suffer strong suppression. Utilizing the experimental PDG average values $\mathcal{B}(\psi \to l^+ l^-)$ [18],

$$\begin{aligned}&\mathcal{B}(J/\psi \to \mu^+\mu^-) = (5.961 \pm 0.033)\%, \\ &\mathcal{B}(\psi(2S) \to l^+ l^-) = \begin{cases} (8.0 \pm 0.6) \times 10^{-3}, & l = \mu, \\ (3.1 \pm 0.4) \times 10^{-3}, & l = \tau, \end{cases} \end{aligned} \quad (34)$$

we have

$$\mathcal{B}_{\rm LD}(\Lambda_b \to \Lambda l^+ l^-) = \begin{cases} (4.91^{+2.78}_{-2.12}) \times 10^{-5}, & l = \mu, \\ (1.12^{+0.86}_{-0.54}) \times 10^{-6}, & l = \tau, \end{cases} \quad (35)$$

where we present the results for the μ and τ channels only since the values for the e and μ channels are essentially the same. It is clear that the LD effects in the tau lepton mode are rather smaller than the counterpart for the μ channel because the secondary process $J/\psi \to \tau^+\tau^-$ is kinematically forbidden. Our result for the μ channel is comparable with those in the light-cone sum rules [115], QCD sum rules, the pole model [116], and several supersymmetric scenarios evaluated in Refs. [36,117]. However, the observation is different for the semitauonic process, for which the obtained results from various approaches span a wide range $(0.59\text{–}11) \times 10^{-6}$ [36,115–117]. Future experimental data are expected to verify and distinguish the various results.

IV. CONCLUSION

Thanks to the continuous efforts of the LHC experiment, a large data sample of b hadrons are produced, offering a unique opportunity to study Λ_b weak decay systematically. In this work, we have carefully explored the color-suppressed

baryonic decays $\Lambda_b \to \Lambda J/\psi, \Lambda\psi(2S)$ in the framework of PQCD, for which the decay process is factorized into the calculable hard kernel and universal hadron distribution amplitudes. In light of these improved universal nonperturbative objects, we have calculated some observables related to the decays under consideration including both the factorizable and nonfactorizable contributions. Our main results are summarized as follows:

(I) Five phenomenological models for the LCDAs of the Λ_b baryon have been employed for comparison. It has been found that the form factors at maximum recoil evaluated by employing the QCDSR model, the exponential model, the free-parton model, and the Gagenbauer-1(2) models are of similar magnitude, whereas the numbers from the Gaussian-type are smaller by about 1 order of magnitude. The main reason is that the Gaussian-type model yields a severe suppression at the end point region. The shape parameters in the LCDAs of the Λ baryon in the literature vary drastically, which means that our form factor results were strongly sensitive to different parameter sets. It has been demonstrated that the COZ models may be the most suitable choices to obtain a reasonable estimate under the PQCD formulism within the accuracy of the current work. The obtained two baryonic transition form factors f_1 and g_1 at maximum recoil are in accord with the expectation in the heavy-quark limit and agree well with the existing results in other works within errors.

(II) We have computed four independent complex helicity amplitudes allowed by angular momentum conservation, which are linearly related to the invariant amplitudes. It has been observed that negative-helicity amplitudes dominate, and the relative contributions from the positive ones only amount to a few percent. In PQCD formulism, the nonfactorizable contributions and vertex corrections provide the main sources of the strong phase. The weak phases from the related CKM matrix elements are almost zero to order λ^2; thus, no direct CP violation is expected. Setting one of the phases to zero, another three relative phases have been estimated, and the obtained values fall into the 95% credibility interval reported by LHCb.

(III) With the helicity amplitude results at hand, we can compute some interesting observables such as branching ratios as well as the various measurable asymmetries. Our prediction $\mathcal{B}(\Lambda_b \to \Lambda J/\psi) = 7.75^{+4.08+1.39}_{-3.17-0.96}$ coincides with the CCQM calculation, but $\mathcal{B}(\Lambda_b \to \Lambda\psi(2S))$ is only half of them. The ratio of the two branching ratios is predicted to be $0.47^{+0.02}_{-0.00}$, which is smaller than those from the other approaches and more consistent with the latest average 0.508 ± 0.023. The predicted up-down asymmetries α_b for the two modes in PQCD differ a lot due to the significant nonfactorizable contributions, which are process dependent. Our number for the J/ψ mode is closer to the most probable value reported by LHCb. The predicted asymmetry for the $\psi(2S)$ mode is large in size and can be tested in future experiments. Moreover, we have also calculated the various observable parameters such as α_2, $r_{0,1}$, and γ_0 defined in terms of the linear combinations of normalized squared helicity amplitudes. The obtained results are compatible within uncertainties with the CCQM calculations and the measurement from the LHCb Collaboration.

(IV) We have discussed the long-distance effects arising from the charmonium resonances regions in the semileptonic decay $\Lambda_b \to \Lambda l^+ l^-$ by using the zero width approximation. Our result for the muonic mode is comparable with other predictions, but for the tauonic one, the various predictions including ours have an obvious discrepancy, which should be clarified in the future.

In brief, the PQCD formalism could be well applied to the concerned color-suppressed Λ_b decays, although our theoretical predictions are still plagued by larger uncertainties due to the hadronic parameters. Some of the obtained observables are compatible with the current data and other theoretical predictions, while others could be measured in the ongoing experiments with certain precision.

ACKNOWLEDGMENTS

We thank Hsiang-nan Li, Fu-Sheng Yu, Yue-Long Shen, and Ya Li for helpful discussions. This work is supported by National Natural Science Foundation of China under Grants No. 12075086 and No. 11605060 and the Natural Science Foundation of Hebei Province under Grants No. A2021209002 and No. A2019209449.

APPENDIX A: VARIOUS LCDA MODELS OF THE Λ_b BARYON

We collect the five widely used parametrized models for the LCDAs of the Λ_b baryon as follows:

(i) Exponential model [59]

$$\Psi_2(x_2, x_3) = x_2 x_3 \frac{M^4}{\omega_0^4} e^{-\frac{\omega}{\omega_0}},$$
$$\Psi_3^{+-}(x_2, x_3) = 2x_2 \frac{M^3}{\omega_0^3} e^{-\frac{\omega}{\omega_0}},$$
$$\Psi_3^{-+}(x_2, x_3) = 2x_3 \frac{M^3}{\omega_0^3} e^{-\frac{\omega}{\omega_0}},$$
$$\Psi_4(x_2, x_3) = \frac{M^2}{\omega_0^2} e^{-\frac{\omega}{\omega_0}}, \tag{A1}$$

with $\omega = (x_2 + x_3)M$ and $\omega_0 = 0.4 \pm 0.1$ GeV.

(ii) Free-parton approximation [59]

$$\Psi_2(x_2,x_3)=\frac{15x_2x_3M^4(2\bar{\Lambda}-\omega)}{4\bar{\Lambda}^5}\Theta(2\bar{\Lambda}-\omega),$$
$$\Psi_3^{+-}(x_2,x_3)=\frac{15x_2M^3(2\bar{\Lambda}-\omega)^2}{4\bar{\Lambda}^5}\Theta(2\bar{\Lambda}-\omega),$$
$$\Psi_3^{-+}(x_2,x_3)=\frac{15x_3M^3(2\bar{\Lambda}-\omega)^2}{4\bar{\Lambda}^5}\Theta(2\bar{\Lambda}-\omega),$$
$$\Psi_4(x_2,x_3)=\frac{5M^2(2\bar{\Lambda}-\omega)^3}{8\bar{\Lambda}^5}\Theta(2\bar{\Lambda}-\omega), \quad \text{(A2)}$$

with $\bar{\Lambda}\equiv(M-m_b)/2\approx 0.8$ GeV.

(iii) Gegenbauer-1 model [58]

$$\Psi_2(x_2,x_3)=M^4x_2x_3 \times\left[\frac{1}{\varepsilon_0^4}e^{-\frac{\omega}{\varepsilon_0}}+\frac{a_2}{\varepsilon_1^4}C_2^{3/2}\left(\frac{x_2-x_3}{x_2+x_3}\right)e^{-\frac{\omega}{\varepsilon_1}}\right],$$
$$\Psi_3^{+-}(x_2,x_3)=2M^3x_2\frac{1}{\varepsilon_3^3}e^{-\frac{\omega}{\varepsilon_3}},$$
$$\Psi_3^{-+}(x_2,x_3)=2M^3x_3\frac{1}{\varepsilon_3^3}e^{-\frac{\omega}{\varepsilon_3}},$$
$$\Psi_4(x_2,x_3)=5M^2\mathcal{N}^{-1}\int_{\frac{\omega}{2}}^{s_0}dse^{-s/\tau}\left(s-\frac{\omega}{2}\right)^3, \quad \text{(A3)}$$

with the constant $\mathcal{N}=\int_0^{s_0}dss^5e^{-s/\tau}$ and other parameters $0.4<\tau<0.8$ GeV, $s_0=1.2$ GeV, $a_2=0.333^{+0.250}_{-0.333}$, $\varepsilon_0=200^{+130}_{-60}$ MeV, $\varepsilon_1=650^{+650}_{-300}$ MeV, and $\varepsilon_3=230$ MeV.

(iv) Gegenbauer-2 model [57]

$$\Psi_2(x_2,x_3)=M^4x_2x_3\sum_{n=0}^{2}\frac{a_n^{(2)}}{\varepsilon_n^{(2)4}}C_n^{3/2}\left(\frac{x_2-x_3}{x_2+x_3}\right)e^{-\frac{\omega}{\varepsilon_n^{(2)}}},$$
$$\Psi_3^{+-}(x_2,x_3)=M^3(x_2+x_3)\left[\sum_{n=0}^{2}\frac{a_n^{(3)}}{\varepsilon_n^{(3)3}}C_n^{1/2}\left(\frac{x_2-x_3}{x_2+x_3}\right)e^{-\frac{\omega}{\varepsilon_n^{(3)}}}+\sum_{n=0}^{3}\frac{b_n^{(3)}}{\eta_n^{(3)3}}C_n^{1/2}\left(\frac{x_2-x_3}{x_2+x_3}\right)e^{-\frac{\omega}{\eta_n^{(3)}}}\right],$$
$$\Psi_3^{-+}(x_2,x_3)=M^3(x_2+x_3)\left[\sum_{n=0}^{2}\frac{a_n^{(3)}}{\varepsilon_n^{(3)3}}C_n^{1/2}\left(\frac{x_2-x_3}{x_2+x_3}\right)e^{-\frac{\omega}{\varepsilon_n^{(3)}}}-\sum_{n=0}^{3}\frac{b_n^{(3)}}{\eta_n^{(3)3}}C_n^{1/2}\left(\frac{x_2-x_3}{x_2+x_3}\right)e^{-\frac{\omega}{\eta_n^{(3)}}}\right],$$
$$\Psi_4(x_2,x_3)=M^2\sum_{n=0}^{2}\frac{a_n^{(4)}}{\varepsilon_n^{(4)2}}C_n^{1/2}\left(\frac{x_2-x_3}{x_2+x_3}\right)e^{-\frac{\omega}{\varepsilon_n^{(4)}}}, \quad \text{(A4)}$$

with the Gegenbauer polynomials

$$C_0^{\xi}(x)=1,\quad C_1^{\xi}(x)=2\xi x,\quad C_2^{\xi}(x)=2\xi(1+\xi)x^2-\xi. \quad \text{(A5)}$$

The relevant parameters for the Gegenbauer-2 model can be found in [57].

(v) QCDSR model [58]

$$\Psi_2(x_2,x_3)=\frac{15}{2\mathcal{N}}M^4x_2x_3\int_{\frac{\omega}{2}}^{s_0}dse^{-s/\tau}\left(s-\frac{\omega}{2}\right),$$
$$\Psi_3^{+-}(x_2,x_3)=\frac{15}{\mathcal{N}}M^3x_2\int_{\frac{\omega}{2}}^{s_0}dse^{-s/\tau}(s-\frac{\omega}{2})^2,$$
$$\Psi_3^{-+}(x_2,x_3)=\frac{15}{\mathcal{N}}M^3x_3\int_{\frac{\omega}{2}}^{s_0}dse^{-s/\tau}(s-\frac{\omega}{2})^2,$$
$$\Psi_4(x_2,x_3)=\frac{5}{\mathcal{N}}M^2\int_{\frac{\omega}{2}}^{s_0}dse^{-s/\tau}(s-\frac{\omega}{2})^3. \quad \text{(A6)}$$

The various models above obey the uniform normalization conditions according to the different twists,

$$\int_0^1dx_2dx_3\Psi_2(x_2,x_3)=1,$$
$$\int_0^1dx_2dx_3(\Psi_3^{+-}(x_2,x_3)+\Psi_3^{-+}(x_2,x_3))/4=1,$$
$$\int_0^1dx_2dx_3\Psi_4(x_2,x_3)=1. \quad \text{(A7)}$$

(vi) Gaussian-type [118,119] This model does not distinguish the asymptotic forms of different twists' LCDAs in favor of an unifying Gaussian shape [120]

$$\Phi_{\Lambda_b}(x_1,x_2,x_3)=Nx_1x_2x_3\exp\left[-\frac{1}{2\beta^2}\left(\frac{M^2}{x_1}+\frac{m_q^2}{x_2}+\frac{m_q^2}{x_3}\right)\right], \quad \text{(A8)}$$

with the normalized constant $N = 6.67 \times 10^{12}$ and shape parameters $\beta = 1.0$ GeV and $m_q = 0.3$ GeV. The corresponding Λ_b baryon LCDA can be expressed as

$$(\Psi_{\Lambda_b})_{\alpha\beta\gamma} = \frac{f_{\Lambda_b}}{8\sqrt{2}N_c}[(\not{p} + M)\gamma_5 C]_{\beta\gamma}[\Lambda_b(p)]_\alpha \times \Phi_{\Lambda_b}(x_1, x_2, x_3). \tag{A9}$$

APPENDIX B: FACTORIZATION FORMULAS

Following the conventions in Ref. [56], we provide some details about the factorization formulas in Eq. (20). The formulas of the equivalent diagrams connected by an interchange of two light quarks will not be repeated here. The explicit expressions of $V^{LL,SP}$ are collected in Table VII, where the combinations of the Wilson coefficients a_l including the vertex corrections are defined as

$$a_l = \begin{cases} C_l + \frac{1}{3}C_{l+1} + \frac{\alpha_s}{4\pi}\frac{C_f}{N_c}C_{l+1}\left[-18 - 12ln\left(\frac{t}{m_b}\right) + f_I\right], & l = 1, 3, 9, \\ C_l + \frac{1}{3}C_{l+1} - \frac{\alpha_s}{4\pi}\frac{C_f}{N_c}C_{l+1}\left[-6 - 12ln\left(\frac{t}{m_b}\right) + f_I\right], & l = 5, 7, \end{cases} \tag{B1}$$

with $C_f = (N_c^2 - 1)/(2N_c)$. For the calculation of f_I, the reader is referred to Refs. [6,121] for details.

The virtualities of the internal propagators $t_{A,B,C,D}$ and the hard amplitudes $H_{T_{ij}}$ for each diagram T_{ij} in Fig. 1 are gathered in the Tables VIII and IX, respectively. The expression of $H_{T_{ij}}$ in Table IX is given for A_1^L and A_2^L, where those terms proportional to r_Λ have been neglected for simplicity. The corresponding formulas for B_1^L and B_2^L can be obtained from A_1^L and A_2^L, respectively, by the following replacement:

$$B_1^L = A_1^L|_{\Phi^V \to -\Phi^V, \Phi^A \to -\Phi^A}, \qquad B_2^L = A_2^L|_{\Phi^T \to -\Phi^T}. \tag{B2}$$

The formulas of $A_1^T(B_1^T)$ have the same form as $A_1^L(B_1^L)$ but with $\psi^L \to \psi^V$ and $\psi^t \to \psi^T$.

TABLE VII. The expressions of V^{LL} and V^{SP} in Eq. (20) for each diagram T_{ij}.

ij	V^{LL}	V^{SP}
$a1, a2, a3, a5, b1, b2, b4$	$V_{cb}V_{cs}^*a_1 + V_{tb}V_{ts}^*(a_3 + a_9)$	$V_{tb}V_{ts}^*(a_5 + a_7)$
$a6, a7, b6, b7, c1, c2, d1, d2$	$\frac{1}{3}V_{cb}V_{cs}^*C_2 + \frac{1}{3}V_{tb}V_{ts}^*(C_4 + C_{10})$	$\frac{1}{3}V_{tb}V_{ts}^*(C_6 + C_8)$
$c5, c7, d6$	$V_{cb}V_{cs}^*(\frac{1}{3}C_2 - \frac{1}{4}C_1) + V_{tb}V_{ts}^*[\frac{1}{3}(C_4 + C_{10}) - \frac{1}{4}(C_3 + C_9)]$	$V_{tb}V_{ts}^*[\frac{1}{3}(C_6 + C_8) - \frac{1}{4}(C_5 + C_7)]$

TABLE VIII. The virtualities of the internal gluon $t_{A,B}$ and quark $t_{C,D}$ for each diagram T_{ij} in Fig. 1.

T_{ij}	$\frac{t_A}{M^2}$	$\frac{t_B}{M^2}$	$\frac{t_C}{M^2}$	$\frac{t_D}{M^2}$
T_{a1}	$f^+x_3x_3'$	$f^+(1-x_1)(1-x_1')$	$f^+(1-x_1)x_3'$	$f^+(1-x_1')$
T_{a2}	$f^+x_3x_3'$	$f^+(1-x_1)(1-x_1')$	$f^+(1-x_1')x_3$	$f^+(1-x_1')$
T_{a3}	$f^+x_3x_3'$	$f^+x_2x_2'$	$x_2 + f^+(1-x_2)x_3'$	$f^+(1-x_1')$
T_{a5}	$f^+x_3x_3'$	$f^+x_2x_2'$	$f^+(1-x_2')x_3$	$x_3 + f^+(1-x_3)x_2'$
T_{a6}	$f^+x_3x_3'$	$f^+x_2x_2'$	$r_c^2 + f^+x_3x_3' + r_\Lambda^2x_3'y - f^+(x_3 + x_3')y + y(x_3 - r^2y)$	$x_3 + f^+(1-x_3)x_2'$
T_{a7}	$f^+x_3x_3'$	$f^+x_2x_2'$	$r_c^2 + f^+x_3x_3' + ((f^+ - 1)x_3 + (f^+ - r_\Lambda^2)x_3' - r^2(y-1))(y-1)$	$x_3 + f^+(1-x_3)x_2'$
T_{b1}	$f^+x_3x_3'$	$f^+(1-x_1)(1-x_1')$	$f^+(1-x_1)x_3'$	$f^+(1-x_1)$
T_{b2}	$f^+x_3x_3'$	$f^+(1-x_1)(1-x_1')$	$f^+(1-x_1')x_3$	$f^+(1-x_1)$
T_{b4}	$f^+x_3x_3'$	$f^+x_2x_2'$	$f^+(1-x_1)$	$f^+(1-x_3')x_2$
T_{b6}	$f^+x_3x_3'$	$f^+x_2x_2'$	$r_c^2 + f^+x_3x_3' + r_\Lambda^2x_3'y - f^+(x_3 + x_3')y + y(x_3 - r^2y)$	$f^+(1-x_3')x_2$
T_{b7}	$f^+x_3x_3'$	$f^+x_2x_2'$	$r_c^2 + f^+x_3x_3' + ((f^+ - 1)x_3 + (f^+ - r_\Lambda^2)x_3' - r^2(y-1))(y-1)$	$f^+(1-x_3')x_2$

(Table continued)

TABLE VIII. *(Continued)*

T_{ij}	$\frac{t_A}{M^2}$	$\frac{t_B}{M^2}$	$\frac{t_C}{M^2}$	$\frac{t_D}{M^2}$
T_{c1}	$f^+x_3x_3'$	$f^+(1-x_1)(1-x_1')$	$f^+(1-x_1)x_3'$	$r_c^2+f^+y(x_1+x_1'-2)+y(1-r^2y-x_1)+(f^+(x_1-1)-yr_\Lambda^2)(x_1'-1)$
T_{c2}	$f^+x_3x_3'$	$f^+(1-x_1)(1-x_1')$	$f^+(1-x_1')x_3$	$r_c^2+f^+y(x_1+x_1'-2)+y(1-r^2y-x_1)+(f^+(x_1-1)-yr_\Lambda^2)(x_1'-1)$
T_{c5}	$f^+x_3x_3'$	$f^+x_2x_2'$	$r_c^2+f^+x_3x_3'+r_\Lambda^2x_3'y-f^+(x_3+x_3')y+y(x_3-r^2y)$	$r_c^2+f^+y(x_1+x_1'-2)+y(1-r^2y-x_1)+(f^+(x_1-1)-yr_\Lambda^2)(x_1'-1)$
T_{c7}	$f^+x_3x_3'$	$f^+x_2x_2'$	$r_c^2+f^+x_3x_3'+((f^+-1)x_3+(f^+-r_\Lambda^2)x_3'-r^2(y-1))(y-1)$	$r_c^2+f^+x_2x_2'+r_\Lambda^2x_2'y-f^+(x_2+x_2')y+y(x_2-r^2y)$
T_{d1}	$f^+x_3x_3'$	$f^+(1-x_1)(1-x_1')$	$f^+(1-x_1)x_3'$	$r_c^2-f^+(y(x_1+x_1'-2)-x_1-x_1'+1)(y-1)(r^2(y-1)-x_1+1-r_\Lambda^2(1-x_1'))$
T_{d2}	$f^+x_3x_3'$	$f^+(1-x_1)(1-x_1')$	$f^+(1-x_1')x_3$	$r_c^2-f^+(y(x_1+x_1'-2)-x_1-x_1'+1)(y-1)(r^2(y-1)-x_1+1-r_\Lambda^2(1-x_1'))$
T_{d6}	$f^+x_3x_3'$	$f^+x_2x_2'$	$r_c^2-f^+(y(x_1+x_1'-2)-x_1-x_1'+1)(y-1)(r^2(y-1)-x_1+1-r_\Lambda^2(1-x_1'))$	$r_c^2+f^+x_3x_3'+((f^+-1)x_3+(f^+-r_\Lambda^2)x_3'-r^2(y-1))(y-1)$

TABLE IX. The expressions of $H_{R_{ij}}^{LL,SP}$ for A_1^L and A_2^L.

	$\frac{A_1^L}{16M^4}$	$\frac{A_2^L}{16M^4}$
$H_{T_{a1}}^{LL(SP)}$	$[-2r(1-r^2)^2x_3'\Psi_4\psi^L]\Phi^A$	$[2r(1-r^2)(x_1-1)(x_1'-1)\psi^L(\Psi_3^{-+}+\Psi_3^{+-})]\Phi^T$
$H_{T_{a2}}^{LL(SP)}$	$[2r(r^2-1)x_3\Psi_4\psi^L]\Phi^A$	$[4r(1-r^2)x_3(x_1'-1)\psi^L\Psi_4]\Phi^A$
$H_{T_{a3}}^{LL(SP)}$	$[r(r^2-1)((r^2-1)x_3'-x_2)\Psi_4\psi^L]\Phi^V+[r(r^2-1)(((r^2-1)x_3'-x_2)\Psi_4+2(1-x_2)\Psi_2)\psi^L]\Phi^A$	$[2r(2(1-r^2)x_3'-x_2(r^2(x_1'-1)-x_1'-1))\psi^L\Psi_4]\Phi^V+[2r(r^2-1)x_2(x_1'-1)\psi^L\Psi_4]\Phi^A+[2r(((1-x_2)(r^2(x_1'-1)-x_1')+1)\Psi_3^{-+}+x_2\Psi_3^{+-})\psi^L]\Phi^T$
$H_{T_{a5}}^{LL(SP)}$	$[r(r^2-1)x_3\Psi_3^{+-}\psi^L]\Phi^T$	$[-2r^3x_3^2\psi^L\Psi_4]\Phi^V+[-2r^3x_3^2\psi^L\Psi_4]\Phi^A+[-2rx_3(r^2(x_3-1)+1)\psi^L\Psi_3^{+-}]\Phi^T$
$H_{T_{a6}}^{LL}$	$[2r(r^2-1)(x_3-1)(x_3-y)\psi^L\Psi_2]\Phi^A+[(1-r^2)(r_c\psi^t+r\psi^L(x_3-y))\Psi_3^{+-}]\Phi^T$	$[2r^2x_3(r_c\psi^t+r\psi^L(x_3-y))\Psi_4]\Phi^V+[2rx_3(rr_c\psi^t\Psi_4+(r^2\Psi_4-2\Psi_2)(x_3-y)\psi^L)]\Phi^A+[2(r^2(x_3-1)+1)(r_c\psi^t+r\psi^L(x_3-y))\Psi_3^{+-}+2r(r^2-1)(x_3-y)x_2'\psi^L\Psi_3^{-+}]\Phi^T$
$H_{T_{a6}}^{SP}$	$[-(1-r^2)^2x_2'(r_c\psi^t+r\psi^L(x_3-y))\Psi_4]\Phi^V+[(r^2-1)^2x_2'(r_c\psi^t+r\psi^L(x_3-y))\Psi_4-2(r^2-1)(x_3-1)r_c\psi^t\Psi_2]\Phi^A$	$[-2(r_c\psi^t(r^2(x_3-x_2')+x_2')+r\psi^L(r^2y(x_2'-x_3)+(r^2-1)x_3(x_3'-x_2')-yx_2'))\Psi_4]\Phi^V+[4((x_3-1)r_c\psi^t+r\psi^L(y-x_3))\Psi_2+2(r\psi^L((r^2-1)yx_2'+r^2x_3y-(r^2-1)x_3(x_2'+x_3'))-r_c\psi^t(r^2(x_2'+x_3)-x_2'))\Psi_4]\Phi^A+[-2r((x_3-1)(rr_c\psi^t+\psi^L((r^2-1)x_3'-r^2y))\Psi_3^{+-}-(r^2-1)(x_3-y)x_2'\psi^L\Psi_3^{-+})]\Phi^T$
$H_{T_{a7}}^{LL}$	$[(r^2-1)^2x_2'(r_c\psi^t+r\psi^L(x_3+y-1))\Psi_4]\Phi^V+[-(1-r^2)^2x_2'(r_c\psi^t+r\psi^L(x_3+y-1))\Psi_4+2(r^2-1)(x_3-1)r_c\psi^t\Psi_2]\Phi^A$	$[2(r_c\psi^t(r^2(x_3-x_2')+x_2')-r\psi^L((r^2-1)(x_3+y-1)x_2'+x_3(x_3'-r^2(x_3'+y-1))))\Psi_4]\Phi^V+[2(r_c(r^2(x_2'+x_3)-x_2')\psi^t+r(r^2x_3(x_3'+y-1)+(r^2-1)(x_3+y-1)x_2'-x_3x_3')\psi^L)\Psi_4+4(r\psi^L(x_3+y-1)-(x_3-1)r_c\psi^t)\Psi_2]\Phi^A+[2r((x_3-1)(rr_c\psi^t+\psi^L(r^2(x_3'+y-1)-x_3'))\Psi_3^{+-}-(r^2-1)(x_3+y-1)x_2'\psi^L\Psi_3^{-+})]\Phi^T$

(Table continued)

TABLE IX. *(Continued)*

	$\frac{A_1^L}{16M^4}$	$\frac{A_2^L}{16M^4}$
$H^{SP}_{T_{a7}}$	$[2r(r^2-1)(1-x_3)(x_3+y-1)\psi^L\Psi_2]\Phi^A+$ $[(r^2-1)(r_c\psi^t+r\psi^L(x_3+y-1))\Psi_3^{+-}]\Phi^T$	$[-2r^2x_3(r_c\psi^t+r\psi^L(x_3+y-1))\Psi_4]\Phi^V+$ $[2rx_3(\psi^L(2\Psi_2-r^2\Psi_4)(x_3+y-1)-rr_c\psi^t\Psi_4)]\Phi^A+$ $[2r(1-r^2)(x_3+y-1)x_2'\psi^L\Psi_3^{-+}-$ $2(r^2(x_3-1)+1)(r_c\psi^t+r\psi^L(x_3+y-1))\Psi_3^{+-}]\Phi^T$
$H^{LL(SP)}_{T_{b1}}$	$[r(1-r^2)(x_1-1)^2(\Psi_3^{-+}+\Psi_3^{+-})\psi^L]\Phi^T$	$[2r(1-r^2)(x_1-1)^2\psi^L(\Psi_3^{-+}+\Psi_3^{+-})]\Phi^T$
$H^{LL(SP)}_{T_{b2}}$	$[-2r(1-r^2)^2x_3\Psi_4\psi^L]\Phi^A$	0
$H^{LL(SP)}_{T_{b4}}$	$[-r(1-r^2)^2x_2\Psi_4\psi^L]\Phi^V+[r(r^2-1)^2x_2\Psi_4\psi^L]\Phi^A+$ $[r(r^2-1)(1-x_1)x_2\Psi_3^{-+}\psi^L]\Phi^T$	$[2r(r^2-1)(1-x_1)x_2\psi^L\Psi_3^{-+}]\Phi^T$
$H^{LL}_{T_{b6}}$	$[r(r^2-1)x_2(rr_c\psi^t+\psi^L((r^2-1)x_3'-r^2y))\Psi_4]\Phi^V+$ $[r(1-r^2)x_2(rr_c\psi^t+\psi^L((r^2-1)x_3'-r^2y))\Psi_4]\Phi^A+$ $[(1-r^2)x_2r_c\psi^t\Psi_3^{-+}]\Phi^T$	$[2(1-r^2)x_2r_c\psi^t\Psi_3^{-+}]\Phi^T$
$H^{SP}_{T_{b6}}$	$[r(r^2-1)x_2(x_3-y)\psi^L\Psi_3^{-+}]\Phi^T$	$[-2r^2x_2(r_c\psi^t+r\psi^L(x_3-y))\Psi_4]\Phi^V+$ $[2r^2x_2(r_c\psi^t+r\psi^L(x_3-y))\Psi_4]\Phi^A+$ $[-2rx_2(rr_c\psi^t+\psi^L(x_3-y))\Psi_3^{-+}]\Phi^T$
$H^{LL}_{T_{b7}}$	$[r(1-r^2)x_2(x_3+y-1)\psi^L\Psi_3^{-+}]\Phi^T$	$[2r^2x_2(r_c\psi^t+r\psi^L(x_3+y-1))\Psi_4]\Phi^V+$ $[-2r^2x_2(r_c\psi^t+r\psi^L(x_3+y-1))\Psi_4]\Phi^A+$ $[2rx_2(rr_c\psi^t+\psi^L(x_3+y-1))\Psi_3^{-+}]\Phi^T$
$H^{SP}_{T_{b7}}$	$[r(1-r^2)x_2(rr_c\psi^t+\psi^L(r^2(x_3'+y-1)-x_3'))\Psi_4]\Phi^V+$ $[r(r^2-1)x_2(rr_c\psi^t+\psi^L(r^2(x_3'+y-1)-x_3'))\Psi_4]\Phi^A+$ $[(r^2-1)x_2r_c\psi^t\Psi_3^{-+}]\Phi^T$	$[2(r^2-1)x_2r_c\psi^t\Psi_3^{-+}]\Phi^T$
$H^{LL}_{T_{c1}}$	$[-2r(1-r^2)^2(x_1+y-1)x_3'\psi^L\Psi_4]\Phi^A+$ $[(r^2-1)(x_1-1)(r\psi^L(x_1+y-1)-r_c\psi^t)(\Psi_3^{-+}+\Psi_3^{+-})]\Phi^T$	$[2(r^2-1)(x_1-1)(r\psi^L(x_1+y-1)-r_c\psi^t)(\Psi_3^{-+}+\Psi_3^{+-})]\Phi^T$
$H^{SP}_{T_{c1}}$	$[-2(1-r^2)^2r_cx_3'\psi^t\Psi_4]\Phi^A$	$[4(1-r^2)x_3'(r\psi^L(x_1+y-1)-r_c\psi^t)\Psi_4]\Phi^A+$ $[2r(1-x_1)(\psi^L(r^2(x_1'+y-1)-x_1'+1)-$ $rr_c\psi^t)(\Psi_3^{-+}+\Psi_3^{+-})]\Phi^T$
$H^{LL}_{T_{c2}}$	$[2r^2(r^2-1)x_3r_c\psi^t\Psi_4]\Phi^A$	0
$H^{SP}_{T_{c2}}$	$[2r(r^2-1)x_3(r^2(x_1'+y-1)-x_1'+1)\psi^L\Psi_4]\Phi^A$	$[-4rx_3(\psi^L(r^2(x_1'+y-1)-x_1'+1)-rr_c\psi^t)\Psi_4]\Phi^A$
$H^{LL}_{T_{c5}}$	$[r(r^2-1)((r_c^2-(x_1+y-1)((1-r^2)x_3'+r^2y))\psi^L-$ $rr_cx_2\psi^t)\Psi_4]\Phi^V+[r(1-r^2)((\psi^L(r_c^2-$ $(x_1+y-1)((1-r^2)x_3'+r^2y))-rr_cx_2\psi^t)\Psi_4+$ $2(r^2-1)(x_1+y-1)(x_3-y)\psi^L\Psi_2)]\Phi^A+$ $[(r^2-1)(1-x_1-y)(r_c\psi^t+r\psi^L(x_3-y))\Psi_3^{+-}+$ $(r^2-1)r_cx_2\psi^t\Psi_3^{-+}]\Phi^T$	$[2(1-r^2)((x_1+y-1)(r_c\psi^t+r\psi^L(x_3-y))\Psi_3^{+-}-$ $r_cx_2\psi^t\Psi_3^{-+})]\Phi^T$
$H^{SP}_{T_{c5}}$	$[(r(r^2-1)\psi^L(r_c^2+(x_3-y)(r^2(x_1'+y-1)-x_1'+1))-$ $(r^2-1)r_cx_2'\psi^t)\Psi_4]\Phi^V+[(1-r^2)((r\psi^L(r_c^2+$ $(x_3-y)(r^2(x_1'+y-1)-x_1'+1))-(r^2-1)r_c\psi^tx_2')\Psi_4+$ $2(r^2-1)r_c(x_3-y)\psi^t\Psi_2)]\Phi^A$	$[-2(r\psi^L(2r_c^2-(r^2-1)(x_3-y)x_2'+$ $(x_2+2x_3-2y)((1-r^2)x_3'+r^2y))+$ $r_c\psi^t(x_2'-r^2(x_2'+x_2)))\Psi_4]\Phi^V+$ $[2(r_c\psi^t(r^2(x_2-x_2')+x_2')-r\psi^L(r^2x_2(y-x_3')+$ $(r^2-1)(x_3-y)x_2'+x_2x_3'))\Psi_4+$ $4(x_3-y)(r_c\psi^t+r\psi^L(x_2+x_3-y))\Psi_2]\Phi^A+$ $[-2r((r_c^2+(x_3-y)(r^2(x_1'+y-1)-x_1'+1))\psi^L\Psi_3^{-+}+$ $r_c(r_c\psi^L+r\psi^t(x_3-y))\Psi_3^{+-})]\Phi^T$
$H^{LL}_{T_{c7}}$	$[2(r^2-1)r_c(x_2-y)\psi^t\Psi_2]\Phi^A+$ $[(r^2-1)(1-x_3-y)(r\psi^L(y-x_2)-r_c\psi^t)\Psi_3^{-+}]\Phi^T$	$[2r\Psi_4(\psi^L(r^2(x_3+y-1)(y-x_2)-r_c^2)+rx_1r_c\psi^t)]\Phi^V+$ $[2r(\psi^L(r_c^2+r^2(x_2-y)(x_3+y-1))-rx_1r_c\psi^t)\Psi_4-$ $4(x_2-y)(r_c\psi^t+r\psi^L(x_3+y-1))\Psi_2]\Phi^A+$ $[2r(x_2-y)(rr_c\psi^t+\psi^L(r^2(x_3'+y-1)-x_3'))\Psi_3^{+-}-$ $2(r\psi^L(r_c^2+(x_2-y)(x_3+y-1))+$ $r_c\psi^t(r^2(x_2-y)+x_3+y-1))\Psi_3^{-+}]\Phi^T$

(Table continued)

TABLE IX. *(Continued)*

	$\frac{A_1^L}{16M^4}$	$\frac{A_2^L}{16M^4}$
$H_{T_{c7}}^{SP}$	$[2(r^2-1)r_c(x_3+y-1)\psi^t\Psi_2]\Phi^A+$ $[(r^2-1)(y-x_2)(r_c\psi^t+r\psi^L(x_3+y-1))\Psi_3^{+-}]\Phi^T$	$[-2r\Psi_4(\psi^L(r^2(x_3+y-1)(y-x_2)-r_c^2)+rx_1r_c\psi^t)]\Phi^V+$ $[-2(r(\psi^L(-(r_c^2+r^2(x_2-y)(x_3+y-1)))+$ $rx_1r_c\psi^t)\Psi_4+2(x_3+y-1)(r_c\psi^t+r\psi^L(x_2-y))\Psi_2)]\Phi^A+$ $[2(r(x_3+y-1)(\psi^L(x_2'-r^2x_2'+r^2y)-rr_c\psi^t)\Psi_3^{-+}+$ $(r\psi^L(r_c^2+(x_2-y)(x_3+y-1))+r_c\psi^t(r^2(x_3+y-1)+$ $x_2-y))\Psi_3^{+-})]\Phi^T$
$H_{T_{d1}}^{LL}$	$[2(r^2-1)^2r_cx_3'\psi^t\Psi_4]\Phi^A$	$[4(r^2-1)x_3'(r\psi^L(x_1-y)-r_c\psi^t)\Psi_4]\Phi^A+$ $[2r(x_1-1)(\psi^L((r^2-1)x_1'-r^2y+1)-rr_c\psi^t)(\Psi_3^{-+}+\Psi_3^{+-})]\Phi^T$
$H_{T_{d1}}^{SP}$	$[2r(r^2-1)^2(x_1-y)x_3'\psi^L\Psi_4]\Phi^A+$ $[(r^2-1)(1-x_1)(r\psi^L(x_1-y)-r_c\psi^t)(\Psi_3^{-+}+\Psi_3^{+-})]\Phi^T$	$[2(1-r^2)(x_1-1)(r\psi^L(x_1-y)-r_c\psi^t)(\Psi_3^{-+}+\Psi_3^{+-})]\Phi^T$
$H_{T_{d2}}^{LL}$	$[2r(1-r^2)x_3((r^2-1)x_1'-r^2y+1)\psi^L\Psi_4]\Phi^A$	$[4rx_3(\psi^L((r^2-1)x_1'-r^2y+1)-rr_c\psi^t)\Psi_4]\Phi^A$
$H_{T_{d2}}^{SP}$	$[2(1-r^2)r^2x_3r_c\psi^t\Psi_4]\Phi^A$	0
$H_{T_{d6}}^{LL}$	$[(r(r^2-1)\psi^L(-r_c^2-(1-x_2-y)(x_1'-$ $r^2(x_1'-y)-1))+(r^2-1)r_c\psi^tx_3')\Psi_4]\Phi^V+$ $[(r^2-1)(r\psi^L((x_2+y-1)(r^2(+y-x_1')-$ $x_2'-x_3')-r_c^2)+(r^2-1)r_c\psi^tx_3')\Psi_4-$ $2(r^2-1)r_c\psi^t(x_2+y-1)\Psi_2]\Phi^A$	$[-2(r\psi^L(-2r_c^2+r^2((x_3+2y-2)x_2'+$ $(y-1)(x_3'+x_3+2y-2)+x_2(x_2'-x_1'+2y-1))-$ $(x_2-x_1+2y-1)x_2'-(x_2+y)x_3'+x_3')+$ $r_c\psi^t(r^2(x_3'+x_3)-x_3'))\Psi_4]\Phi^V+$ $[2(r_c\psi^t(r^2(x_3-x_3')+x_3')+r\psi^L(r^2(x_3(x_2'+y-1)-$ $(x_2+y-1)x_3')+(x_2+y-1)x_3'-x_3x_2'))\Psi_4+$ $4(x_2+y-1)(r_c\psi^t+r\psi^L(y-x_1))\Psi_2]\Phi^A+$ $[2r(r_c^2\psi^L(\Psi_3^{-+}+\Psi_3^{+-})-rr_c\psi^t(x_1+x_3-y)\Psi_3^{-+}+$ $\psi^L(x_1+x_3-y)(r^2y+x_1'(1-r^2)-1)\Psi_3^{+-})]\Phi^T$
$H_{T_{d6}}^{SP}$	$[r(r^2-1)(\psi^L(-r_c^2-(x_1-y)(r^2(y-x_3')-$ $r^2x_1'-x_2'))+rx_3r_c\psi^t)\Psi_4]\Phi^V+$ $[r(r^2-1)((\psi^L((y-x_1)(r^2(x_2'+y-1)-x_2')-r_c^2)+$ $rx_3r_c\psi^t)\Psi_4+2(r^2-1)(x_2+y-1)(y-x_1)\psi^L\Psi_2)]\Phi^A+$ $[(1-r^2)((x_1-y)(r\psi^L(x_1+x_3-y)-r_c\psi^t)\Psi_3^{-+}+$ $(r^2-1)x_3r_c\psi^t\Psi_3^{+-})]\Phi^T$	$[2(1-r^2)((x_1-y)(r\psi^L(1-x_2-y)-r_c\psi^t)\Psi_3^{-+}+$ $x_3r_c\psi^t\Psi_3^{+-})]\Phi^T$

[1] M. Neubert and A. A. Petrov, Comments on color suppressed hadronic B decays, Phys. Lett. B **519**, 50 (2001).

[2] F. Abe *et al.* (CDF Collaboration), Reconstruction of $B^0 \to J/\psi K_s^0$ and Measurement of Ratios of Branching Ratios Involving $B \to J/\psi K^*$, Phys. Rev. Lett. **76**, 2015 (1996).

[3] K. Abe *et al.* (Belle Collaboration), Measurement of branching fractions and charge asymmetries for two-body B meson decays with charmonium, Phys. Rev. D **67**, 032003 (2003).

[4] B. Aubert *et al.* (*BABAR* Collaboration), Measurement of Branching Fractions and Charge Asymmetries for Exclusive B Decays to Charmonium, Phys. Rev. Lett. **94**, 141801 (2005).

[5] C. H. Chen and H. N. Li, Nonfactorizable contributions to B meson decays into charmonia, Phys. Rev. D **71**, 114008 (2005).

[6] H. Y. Cheng and K. C. Yang, $B \to J/\psi K$ decays in QCD factorization, Phys. Rev. D **63**, 074011 (2001).

[7] G. Buchalla, A. J. Buras, and M. E. Lautenbacher, Weak decays beyond leading logarithms, Rev. Mod. Phys. **68**, 1125 (1996).

[8] T. Mannel and S. Recksiegel, Probing the helicity structure of $b \to s\gamma$ in $\Lambda_b \to \Lambda\gamma$, Acta Phys. Pol. B **28**, 2489 (1997), https://inspirehep.net/literature/449501.

[9] G. Hiller, M. Knecht, F. Legger, and T. Schietinger, Photon polarization from helicity suppression in radiative decays of polarized Λ_b to spin 3/2 baryons, Phys. Lett. B **649**, 152 (2007).

[10] C. Albajar *et al.* (UA1 Collaboration), First observation of the beauty baryon Λ_b in the decay channel $\Lambda_b \to J/\psi\Lambda$ at the CERN proton-anti-proton collider, Phys. Lett. B **273**, 540 (1991).

[11] F. Abe *et al.* (CDF Collaboration), Search for $\Lambda_b \to J/\psi\Lambda^0$ in $p\bar{p}$ collisions at $\sqrt{s} = 1.8$ TeV, Phys. Rev. D **47**, R2639 (1993).

[12] A. Abulencia *et al.* (CDF Collaboration), Measurement of the Λ_b^0 Lifetime in $\Lambda_b^0 \to J/\psi\Lambda^0$ in $p\bar{p}$ Collisions at $\sqrt{s} = 1.96$ TeV, Phys. Rev. Lett. **98**, 122001 (2007).

[13] F. Abe *et al.* (CDF Collaboration), Observation of $\Lambda_b^0 \to J/\psi\Lambda$ at the Fermilab proton antiproton collider, Phys. Rev. D **55**, 1142 (1997).

[14] V. M. Abazov *et al.* (D0 Collaboration), Measurement of the Λ_b^0 Lifetime in the Decay $\Lambda_b^0 \to J/\psi\Lambda^0$ with the D0 Detector, Phys. Rev. Lett. **94**, 102001 (2005).

[15] V. M. Abazov *et al.* (D0 Collaboration), Measurement of the Λ_b Lifetime in the Exclusive Decay $\Lambda_b \to J/\psi\Lambda$, Phys. Rev. Lett. **99**, 142001 (2007).

[16] V. M. Abazov *et al.* (D0 Collaboration), Measurement of the production fraction times branching fraction $f(b \to \Lambda_b) \cdot \mathcal{B}(\Lambda_b \to J/\psi\Lambda)$, Phys. Rev. D **84**, 031102 (2011).

[17] V. M. Abazov *et al.* (D0 Collaboration), Measurement of the Λ_b^0 lifetime in the exclusive decay $\Lambda_b^0 \to J/\psi\Lambda^0$ in $p\bar{p}$ collisions at $\sqrt{s} = 1.96$ TeV, Phys. Rev. D **85**, 112003 (2012).

[18] Particle Data Group, Review of particle physics, Prog. Theor. Exp. Phys. **2020**, 083C01 (2020).

[19] R. Aaij *et al.* (LHCb Collaboration), Measurements of the $\Lambda_b^0 \to J/\psi\Lambda$ decay amplitudes and the Λ_b^0 polarisation in pp collisions at $\sqrt{s} = 7$ TeV, Phys. Lett. B **724**, 27 (2013).

[20] G. Aad *et al.* (ATLAS Collaboration), Measurement of the parity-violating asymmetry parameter α_b and the helicity amplitudes for the decay $\Lambda_b^0 \to J/\psi + \Lambda^0$ with the ATLAS detector, Phys. Rev. D **89**, 092009 (2014).

[21] CMS Collaboration, Measurement of Λ_b polarization and the angular parameters of the decay $\Lambda_b \to \Lambda J/\psi$, Report No. CMS-PAS-BPH-15-002, 2016.

[22] A. M. Sirunyan *et al.* (CMS Collaboration), Measurement of the Λ_b polarization and angular parameters in $\Lambda_b \to J/\psi\Lambda$ decays from pp collisions at $\sqrt{s} = 7$ and 8 TeV, Phys. Rev. D **97**, 072010 (2018).

[23] R. Aaij *et al.* (LHCb Collaboration), Measurement of the $\Lambda_b^0 \to J/\psi\Lambda$ angular distribution and the Λ_b^0 polarisation in pp collisions, J. High Energy Phys. 06 (2020) 110.

[24] R. Aaij *et al.* (LHCb Collaboration), Observation of $\Lambda_b^0 \to \psi(2S)pK^-$ and $\Lambda_b^0 \to J/\psi\pi^+\pi^-pK^-$ decays and a measurement of the Λ_b^0 baryon mass, J. High Energy Phys. 05 (2016) 132.

[25] R. Aaij *et al.* (LHCb Collaboration), Observation of the Decays $\Lambda_b^0 \to \chi_{c1}pK^-$ and $\Lambda_b^0 \to \chi_{c2}pK^-$, Phys. Rev. Lett. **119**, 062001 (2017).

[26] R. Aaij *et al.* (LHCb Collaboration), Observation of the decay $\Lambda_b^0 \to \psi(2S)p\pi^-$, J. High Energy Phys. 08 (2018) 131.

[27] R. Aaij *et al.* (LHCb Collaboration), Observation of the $\Lambda_b^0 \to \chi_{c1}(3872)pK^-$ decay, J. High Energy Phys. 09 (2019) 028.

[28] G. Aad *et al.* (ATLAS Collaboration), Measurement of the branching ratio $\Gamma(\Lambda_b^0 \to \psi(2S)\Lambda^0)/\Gamma(\Lambda_b^0 \to J/\psi\Lambda^0)$ with the ATLAS detector, Phys. Lett. B **751**, 63 (2015).

[29] R. Aaij *et al.* (LHCb Collaboration), Measurement of the ratio of branching fractions of the decays $\Lambda_b^0 \to \psi(2S)\Lambda$ and $\Lambda_b^0 \to J/\psi\Lambda$, J. High Energy Phys. 03 (2019) 126.

[30] A. K. Leibovich, Z. Ligeti, I. W. Stewart, and M. B. Wise, Predictions for nonleptonic Λ_b and Θ_b decays, Phys. Lett. B **586**, 337 (2004).

[31] R. Mohanta, A. K. Giri, M. P. Khanna, M. Ishida, S. Ishida, and M. Oda, Hadronic weak decays of Λ_b baryon in the covariant oscillator quark model, Prog. Theor. Phys. **101**, 959 (1999).

[32] H. Y. Cheng, Nonleptonic weak decays of bottom baryons, Phys. Rev. D **56**, 2799 (1997); Erratum, Phys. Rev. D **99**, 079901 (2019).

[33] Fayyazuddin and Riazuddin, Two-body nonleptonic Λ_b decays in quark model with factorization ansatz, Phys. Rev. D **58**, 014016 (1998).

[34] M. A. Ivanov, J. G. Korner, V. E. Lyubovitskij, and A. G. Rusetsky, Exclusive nonleptonic bottom to charm baryon decays including nonfactorizable contributions, Mod. Phys. Lett. A **13**, 181 (1998).

[35] Z. T. Wei, H. W. Ke, and X. Q. Li, Evaluating decay rates and asymmetries of Λ_b into light baryons in LFQM, Phys. Rev. D **80**, 094016 (2009).

[36] L. Mott and W. Roberts, Rare dileptonic decays of Λ_b in a quark model, Int. J. Mod. Phys. A **27**, 1250016 (2012).

[37] Fayyazuddin and M. J. Aslam, Hadronic weak decay $\mathcal{B}_b(\frac{1}{2}^+) \to \mathcal{B}(\frac{1}{2}^+, \frac{3}{2}^+) + V$, Phys. Rev. D **95**, 113002 (2017).

[38] C. H. Chou, H. H. Shih, S. C. Lee, and H. n. Li, $\Lambda_b \to \Lambda J/\psi$ decay in perturbative QCD, Phys. Rev. D **65**, 074030 (2002).

[39] J. Zhu, Z. T. Wei, and H. W. Ke, Semileptonic and nonleptonic weak decays of Λ_b^0, Phys. Rev. D **99**, 054020 (2019).

[40] M. A. Ivanov, J. G. Korner, V. E. Lyubovitskij, and A. G. Rusetsky, Exclusive nonleptonic decays of bottom and charm baryons in a relativistic three quark model: Evaluation of nonfactorizing diagrams, Phys. Rev. D **57**, 5632 (1998).

[41] H. Y. Cheng and B. Tseng, 1/M corrections to baryonic form-factors in the quark model, Phys. Rev. D **53**, 1457 (1996); Erratum, Phys. Rev. D **55**, 1697 (1997).

[42] Y. K. Hsiao, P. Y. Lin, C. C. Lih, and C. Q. Geng, Charmful two-body anti-triplet b-baryon decays, Phys. Rev. D **92**, 114013 (2015).

[43] T. Gutsche, M. A. Ivanov, J. G. Körner, V. E. Lyubovitskij, V. V. Lyubushkin, and P. Santorelli, Theoretical description of the decays $\Lambda_b \to \Lambda^{(*)}(\frac{1}{2}^{\pm}, \frac{3}{2}^{\pm}) + J/\psi$, Phys. Rev. D **96**, 013003 (2017).

[44] T. Gutsche, M. A. Ivanov, J. G. Körner, V. E. Lyubovitskij, and P. Santorelli, Polarization effects in the cascade decay in the covariant confined quark model, Phys. Rev. D **88**, 114018 (2013).

[45] T. Gutsche, M. A. Ivanov, J. G. Körner, V. E. Lyubovitskij, and P. Santorelli, Towards an assessment of the ATLAS data on the branching ratio, Phys. Rev. D **92**, 114008 (2015).

[46] Z. J. Ajaltouni, E. Conte, and O. Leitner, Λ_b decays into Λ-vector, Phys. Lett. B **614**, 165 (2005).

[47] Y. K. Hsiao, P. Y. Lin, L. W. Luo, and C. Q. Geng, Fragmentation fractions of two-body b-baryon decays, Phys. Lett. B **751**, 127 (2015).

[48] T. Gutsche, M. A. Ivanov, J. G. Körner, and V. E. Lyubovitskij, Nonleptonic two-body decays of single heavy baryons Λ_Q, Ξ_Q, and Ω_Q ($Q = b$, c) induced by W emission in the covariant confined quark model, Phys. Rev. D **98**, 074011 (2018).

[49] Z. P. Xing, F. Huang, and W. Wang, Angular distributions for $\Lambda_b \to \Lambda_J^*(pK^-)J/\psi$ decays, arXiv:2203.13524.

[50] H. H. Shih, S. C. Lee, and H. n. Li, The $\Lambda_b \to p l\bar{\nu}$ decay in perturbative QCD, Phys. Rev. D **59**, 094014 (1999).

[51] H. H. Shih, S. C. Lee, and H. n. Li, Applicability of perturbative QCD to $\Lambda_b \to \Lambda_c$ decays, Phys. Rev. D **61**, 114002 (2000).

[52] H. H. Shih, S. C. Lee, and H. N. Li, Asymmetry parameter in the polarized $\Lambda_b \to \Lambda_c l\bar{\nu}$ decay, Chin. J. Phys. **39**, 328 (2001), https://inspirehep.net/literature/565648.

[53] X. G. He, T. Li, X. Q. Li, and Y. M. Wang, PQCD calculation for $\Lambda_b \to \Lambda\gamma$ in the standard model, Phys. Rev. D **74**, 034026 (2006).

[54] C. D. Lu, Y. M. Wang, H. Zou, A. Ali, and G. Kramer, Anatomy of the pQCD approach to the baryonic decays $\Lambda_b \to p\pi, pK$, Phys. Rev. D **80**, 034011 (2009).

[55] J. J. Han, Y. Li, H. n. Li, Y. L. Shen, Z. J. Xiao, and F. S. Yu, $\Lambda_b \to p$ transition form factors in perturbative QCD, Eur. Phys. J. C **82**, 686 (2022).

[56] C. Q. Zhang, J. M. Li, M. K. Jia, and Z. Rui, Nonleptonic two-body decays of $\Lambda_b \to \Lambda_c\pi, \Lambda_c K$ in the perturbative QCD approach, Phys. Rev. D **105**, 073005 (2022).

[57] A. Ali, C. Hambrock, and A. Y. Parkhomenko, Light-cone wave functions of heavy baryons, Theor. Math. Phys. **170**, 2 (2012).

[58] P. Ball, V. M. Braun, and E. Gardi, Distribution amplitudes of the Λ_b baryon in QCD, Phys. Lett. B **665**, 197 (2008).

[59] G. Bell, T. Feldmann, Y. M. Wang, and M. W. Y. Yip, Light-cone distribution amplitudes for heavy-quark hadrons, J. High Energy Phys. 11 (2013) 191.

[60] Y. M. Wang and Y. L. Shen, Perturbative corrections to $\Lambda_b \to \Lambda$ form factors from QCD light-cone sum rules, J. High Energy Phys. 02 (**2016**) 179.

[61] V. L. Chernyak, A. A. Ogloblin, and I. R. Zhitnitsky, Wave functions of octet baryons, Z. Phys. C **42**, 569 (1989).

[62] Z. Rui and Z. T. Zou, S-wave ground state charmonium decays of B_c mesons in the perturbative QCD approach, Phys. Rev. D **90**, 114030 (2014).

[63] Z. Rui, W. F. Wang, G. x. Wang, L. h. Song, and C. D. Lü, The $B_c \to \psi(2S)\pi$, $\eta_c(2S)\pi$ decays in the perturbative QCD approach, Eur. Phys. J. C **75**, 293 (2015).

[64] Z. Rui, H. Li, G. x. Wang, and Y. Xiao, Semileptonic decays of B_c meson to S-wave charmonium states in the perturbative QCD approach, Eur. Phys. J. C **76**, 564 (2016).

[65] Z. Rui, Y. Li and, and W. F. Wang, The S-wave resonance contributions in the B_s^0 decays into $\psi(2S, 3S)$ plus pion pair, Eur. Phys. J. C **77**, 199 (2017).

[66] Z. Rui, Y. Li, and Z. J. Xiao, Branching ratios, CP asymmetries and polarizations of $B \to \psi(2S)V$ decays, Eur. Phys. J. C **77**, 610 (2017).

[67] Z. Rui and W. F. Wang, S-wave $K\pi$ contributions to the hadronic charmonium B decays in the perturbative QCD approach, Phys. Rev. D **97**, 033006 (2018).

[68] Z. Rui, Y. Li, and H. N. Li, P-wave contributions to $B \to \psi\pi\pi$ decays in perturbative QCD approach, Phys. Rev. D **98**, 113003 (2018).

[69] Z. Rui, Y. Q. Li, and J. Zhang, Isovector scalar $a_0(980)$ and $a_0(1450)$ resonances in the $B \to \psi(K\bar{K}, \pi\eta)$ decays, Phys. Rev. D **99**, 093007 (2019).

[70] Z. Rui, Y. Li, and H. Li, Studies of the resonance components in the B_s decays into charmonia plus kaon pair, Eur. Phys. J. C **79**, 792 (2019).

[71] Y. Li, Z. Rui, and Z. J. Xiao, P-wave contributions to $B_{(s)} \to \psi K\pi$ decays in perturbative QCD approach, Chin. Phys. C **44**, 073102 (2020).

[72] Y. Li, D. C. Yan, Z. Rui, and Z. J. Xiao, S, P and D-wave resonance contributions to $B_{(s)} \to \eta_c(1S, 2S)K\pi$ decays in the perturbative QCD approach, Phys. Rev. D **101**, 016015 (2020).

[73] X. Liu, H. n. Li, and Z. J. Xiao, Improved perturbative QCD formalism for B_c meson decays, Phys. Rev. D **97**, 113001 (2018).

[74] X. Liu, H. n. Li, and Z. J. Xiao, Next-to-leading-logarithm k_T resummation for $B_c \to J/\psi$ decays, Phys. Lett. B **811**, 135892 (2020).

[75] M. Beneke, G. Buchalla, M. Neubert, and C. T. Sachrajda, QCD Factorization for $B \to \pi\pi$ Decays: Strong Phases and CP Violation in the Heavy Quark Limit, Phys. Rev. Lett. **83**, 1914 (1999).

[76] M. Beneke, G. Buchalla, M. Neubert, and C. T. Sachrajda, QCD factorization for exclusive, nonleptonic B meson decays: General arguments and the case of heavy light final states, Nucl. Phys. **B591**, 313 (2000).

[77] M. Beneke and M. Neubert, QCD factorization for $B \to PP$ and $B \to PV$ decays, Nucl. Phys. **B675**, 333 (2003).

[78] A. Ali, C. Hambrock, A. Y. Parkhomenko, and W. Wang, Light-cone distribution amplitudes of the ground state bottom baryons in HQET, Eur. Phys. J. C **73**, 2302 (2013).

[79] V. M. Braun, S. E. Derkachov, and A. N. Manashov, Integrability of the evolution equations for heavy-light baryon distribution amplitudes, Phys. Lett. B **738**, 334 (2014).

[80] S. Groote, J. G. Korner, and O. I. Yakovlev, An analysis of diagonal and nondiagonal QCD sum rules for heavy baryons at next-to-leading order in α_s, Phys. Rev. D **56**, 3943 (1997).

[81] K. S. Huang, W. Liu, Y. L. Shen, and F. S. Yu, $\Lambda_b \to p$, $N^*(1535)$ form factors from QCD light-cone sum rules, arXiv:2205.06095.

[82] G. R. Farrar, H. Zhang, A. A. Ogloblin, and I. R. Zhitnitsky, Baryon wave functions and cross-sections for photon annihilation to baryon pairs, Nucl. Phys. **B311**, 585 (1989).

[83] Y. L. Liu, C. Y. Cui, and M. Q. Huang, Higher order light-cone distribution amplitudes of the Λ baryon, Eur. Phys. J. C **74**, 3041 (2014).

[84] Y. L. Liu and M. Q. Huang, Distribution amplitudes of Σ and Λ and their electromagnetic form factors, Nucl. Phys. **A821**, 80 (2009).

[85] G. S. Bali, V. M. Braun, M. Göckeler, M. Gruber, F. Hutzler, A. Schäfer, R. W. Schiel, J. Simeth, W. Söldner, A. Sternbeck *et al.*, Light-cone distribution amplitudes of the baryon octet, J. High Energy Phys. 02 (2016) 070.

[86] V. M. Braun, S. Collins, B. Gläßle, M. Göckeler, A. Schäfer, R. W. Schiel, W. Söldner, A. Sternbeck, and P. Wein, Light-cone distribution amplitudes of the nucleon and negative parity nucleon resonances from lattice QCD, Phys. Rev. D **89**, 094511 (2014).

[87] G. S. Bali *et al.* (RQCD Collaboration), Light-cone distribution amplitudes of octet baryons from lattice QCD, Eur. Phys. J. A **55**, 116 (2019).

[88] G. T. Bodwin, E. Braaten, and G. P. Lepage, Rigorous QCD analysis of inclusive annihilation and production of heavy quarkonium, Phys. Rev. D **51**, 1125 (1995).

[89] M. Beneke, F. Maltoni, and I. Z. Rothstein, QCD analysis of inclusive B decay into charmonium, Phys. Rev. D **59**, 054003 (1999).

[90] Y. Jia and D. Yang, Refactorizing NRQCD short-distance coefficients in exclusive quarkonium production, Nucl. Phys. **B814**, 217 (2009).

[91] Y. C. Chen and H. n. Li, Three-parton contribution to pion form factor in k_T factorization, Phys. Rev. D **84**, 034018 (2011).

[92] Y. C. Chen and H. N. Li, Three-parton contribution to the $B \to \pi$ form factors in k_T factorization, Phys. Lett. B **712**, 63 (2012).

[93] V. M. Belyaev, V. M. Braun, A. Khodjamirian, and R. Ruckl, $D^*D\pi$ and $B^*B\pi$ couplings in QCD, Phys. Rev. D **51**, 6177 (1995).

[94] J. G. Korner and M. Kramer, Exclusive nonleptonic charm baryon decays, Z. Phys. C **55**, 659 (1992).

[95] J. Botts and G. F. Sterman, Hard elastic scattering in QCD: Leading behavior, Nucl. Phys. **B325**, 62 (1989).

[96] B. Kundu, H. n. Li, J. Samuelsson, and P. Jain, The perturbative proton form-factor reexamined, Eur. Phys. J. C **8**, 637 (1999).

[97] D. Hatton, C. T. H. Davies, B. Galloway, J. Koponen, G. P. Lepage, and A. T. Lytle (HPQCD Collaboration), Charmonium properties from lattice QCD + QED: Hyperfine splitting, J/ψ leptonic width, charm quark mass, and a_μ^c, Phys. Rev. D **102**, 054511 (2020).

[98] H. S. Chung, $\overline{\mathrm{MS}}$ renormalization of S-wave quarkonium wavefunctions at the origin, J. High Energy Phys. 12 (2020) 065.

[99] T. M. Aliev, K. Azizi, and M. Savci, Analysis of the $\Lambda_b \to \Lambda \ell^+ \ell^-$ decay in QCD, Phys. Rev. D **81**, 056006 (2010).

[100] C. S. Huang and H. G. Yan, Exclusive rare decays of heavy baryons to light baryons: $\Lambda(b) \to \Lambda\gamma$ and $\Lambda_b \to \Lambda l^+ l^-$, Phys. Rev. D **59**, 114022 (1999); Erratum, Phys. Rev. D **61**, 039901 (2000).

[101] T. Gutsche, M. A. Ivanov, J. G. Korner, V. E. Lyubovitskij, and P. Santorelli, Rare baryon decays $\Lambda_b \to \Lambda l^+ l^- (l = e, \mu, \tau)$ and $\Lambda_b \to \Lambda\gamma$: Differential and total rates, lepton- and hadron-side forward-backward asymmetries, Phys. Rev. D **87**, 074031 (2013).

[102] R. Mohanta, A. K. Giri, and M. P. Khanna, Charmless two-body hadronic decays of Λ_b baryon, Phys. Rev. D **63**, 074001 (2001).

[103] W. Detmold and S. Meinel, $\Lambda_b \to \Lambda \ell^+ \ell^-$ form factors, differential branching fraction, and angular observables from lattice QCD with relativistic b quarks, Phys. Rev. D **93**, 074501 (2016).

[104] X. Liu, W. Wang, and Y. Xie, Penguin pollution in $B \to J/\psi V$ decays and impact on the extraction of the $B_s - \bar{B}_s$ mixing phase, Phys. Rev. D **89**, 094010 (2014).

[105] P. Astbury, J. Gallivan, J. Jafar, M. Letheren, V. Steiner, J. A. Wilson, W. Beusch, M. Borghini, D. Websdale, L. Fluri *et al.*, Measurement of the differential cross-section and the spin-correlation parameters P, A, and R in the backward peak of $\pi^- p \to K^0\Lambda$ at 5 GeV/c, Nucl. Phys. **B99**, 30 (1975).

[106] W. E. Cleland, G. Conforto, G. H. Eaton, H. J. Gerber, M. Reinharz, A. Gautschi, E. Heer, C. Revillard, and G. Von Dardel, A measurement of the β-parameter in the charged nonleptonic decay of the Λ^0 hyperon, Nucl. Phys. **B40**, 221 (1972).

[107] P. M. Dauber, J. P. Berge, J. R. Hubbard, D. W. Merrill, and R. A. Muller, Production and decay of cascade hyperons, Phys. Rev. **179**, 1262 (1969).

[108] O. E. Overseth and R. F. Roth, Time Reversal Invariance in Λ^0 Decay, Phys. Rev. Lett. **19**, 391 (1967).

[109] J. W. Cronin and O. E. Overseth, Measurement of the decay parameters of the Λ^0 particle, Phys. Rev. **129**, 1795 (1963).

[110] M. Ablikim *et al.* (BESIII Collaboration), Polarization and entanglement in baryon-antibaryon pair production in electron-positron annihilation, Nat. Phys. **15**, 631 (2019).

[111] D. G. Ireland, M. Döring, D. I. Glazier, J. Haidenbauer, M. Mai, R. Murray-Smith, and D. Rönchen, Kaon Photoproduction and the Λ Decay Parameter α_-, Phys. Rev. Lett. **123**, 182301 (2019).

[112] H. Y. Jiang and F. S. Yu, Fragmentation-fraction ratio f_{Ξ_b}/f_{Λ_b} in b- and c-baryon decays, Eur. Phys. J. C **78**, 224 (2018).

[113] M. Galanti, A. Giammanco, Y. Grossman, Y. Kats, E. Stamou, and J. Zupan, Heavy baryons as polarimeters at colliders, J. High Energy Phys. 11 (2015) 067.

[114] O. Leitner, Z. J. Ajaltouni, and E. Conte, An angular distribution analysis of Λ_b decays, Nucl. Phys. **A755**, 435 (2005).

[115] Y. m. Wang, Y. Li, and C. D. Lu, Rare decays of $\Lambda_b \to \Lambda + \gamma$ and $\Lambda_b \to \Lambda + l^+ l^-$ in the light-cone sum rules, Eur. Phys. J. C **59**, 861 (2009).

[116] C. H. Chen and C. Q. Geng, Rare $\Lambda_b \to \Lambda l^+ l^-$ decays with polarized Λ, Phys. Rev. D **63**, 114024 (2001).

[117] M. J. Aslam, Y. M. Wang, and C. D. Lu, Exclusive semileptonic decays of $\Lambda_b \to \Lambda l^+ l^-$ in supersymmetric theories, Phys. Rev. D **78**, 114032 (2008).

[118] W. Loinaz and R. Akhoury, Exclusive semileptonic decays of b baryons into protons, Phys. Rev. D **53**, 1416 (1996).

[119] F. Hussain, J. G. Korner, M. Kramer, and G. Thompson, On heavy baryon decay form-factors, Z. Phys. C **51**, 321 (1991).

[120] F. Schlumpf, Relativistic constituent quark model for baryons, Ph.D. thesis, University of Zurich, Zurich, 1992.

[121] H. Y. Cheng, Y. Y. Keum, and K. C. Yang, $B \to J/\psi K^*$ decays in QCD factorization, Phys. Rev. D **65**, 094023 (2002).